Tectonics

RESEARCH ARTICLE
10.1029/2019TC005708

Deep Crustal Flow Within Postorogenic Metamorphic Core Complexes: Insights From the Southern Western Gneiss Region of Norway

J. D. Wiest[1], P. T. Osmundsen[2,3], J. Jacobs[1], and H. Fossen[5]

[1]Department of Earth Science, University of Bergen, Bergen, Norway, [2]Department of Geoscience and Petroleum, Norwegian University of Science and Technology, Trondheim, Norway, [3]Department of Geosciences, University of Oslo, Oslo, Norway, [4]Museum of Natural History and Department of Earth Science, University of Bergen, Bergen, Norway

Key Points:
- A deeply eroded and particularly well-exposed transtensional core complex reveals mechanisms of solid-state viscous flow in the deep crust
- Vertical metamorphic variations and lateral strain gradients lead to differential folding of distinct crustal levels
- Solid-state flow mechanisms are similar to anatectic crust and can contribute to postorogenic exhumation of (ultra-)high-pressure rocks

Correspondence to:
J. D. Wiest,
johannes.wiest@uib.no

Citation:
Wiest, J. D., Osmundsen, P. T., Jacobs, J., & Fossen, H. (2019). Deep Crustal Flow Within Postorogenic Metamorphic Core Complexes: Insights From the Southern Western Gneiss Region of Norway. *Tectonics*, *38*. 4267–4289. https://doi.org/10.1029/2019TC005708

Received 5 JUN 2019
Accepted 6 NOV 2019
Accepted article online 11 NOV 2019
Published online 17 DEC 2019

Abstract Viscous crustal flow can exhume once deeply buried rocks in postorogenic metamorphic core complexes (MCCs). While migmatite domes record the flow dynamics of anatectic crust, the mechanics and kinematics of solid-state flow in the deep crust are poorly constrained. To address this issue, we studied a deeply eroded and particularly well-exposed MCC in the southern Western Gneiss Region of Norway. The Gulen MCC formed during Devonian transtensional collapse of the Caledonian orogeny in the footwall of the Nordfjord-Sogn detachment zone. We developed a semiquantitative mapping scheme for ductile strain to constrain micro- to megascale processes, which brought eclogite-bearing crust from the orogenic root into direct contact with Devonian supradetachment basins. The Gulen MCC comprises different structural levels with distinct metamorphic evolutions. In the high-grade core, amphibolite-facies structures record fluid-controlled eclogite retrogression and coaxial flow involving vast extension-perpendicular shortening. Detachment mylonites formed during ductile-to-brittle noncoaxial deformation and wrap around the core. We present a sequential 3-D reconstruction of MCC formation. In the detachment zone, the combined effects of simple shearing, incision/excision, and erosion thinned the upper crust. Internal necking of the ductile crust was compensated by extension-perpendicular shortening within the deep crust and resulted in differential folding of distinct crustal levels. We identify this differential folding as the main mechanism that can redistribute material within solid-state MCCs. Our interpretation suggests a continuum of processes from migmatite-cored to solid-state MCCs and has implications for postorogenic exhumation of (ultra-)high-pressure rocks.

Plain Language Summary The Earth's crust has different layers with contrasting mechanics. Rocks in the upper crust tend to break, while higher temperatures at depth make rocks flow, although very slowly. This contrast is important when continents collide forming mountain belts but also when plates drift apart and mountain ranges collapse. In SW Norway, hundreds of million years of erosion have exposed rocks that once were deep below a large mountain range (the Caledonides). Today, glacier-polished fjords reveal large dome structures that formed when the Caledonides collapsed. Inside such a dome, we find rocks originating from different levels of the crust. Rocks and structures in the core formed at high pressures and temperatures. Wrapped around, we find rocks that deformed while they cooled down, became more resistant to flow, and finally broke apart. Above the dome, we find remnants of the upper crust, which was broken up by faults, eroded, and deposited in sedimentary basins. We reconstruct how mechanical contrasts between crustal layers brought rocks from the root of the mountain belt in contact with sediments deposited at the surface. Understanding this process is important, because it can entirely transform the crust within a—geologically speaking—short period of time.

1. Introduction

Postorogenic metamorphic core complexes (MCCs) show that the crust reequilibrates after orogeny and an entirely new crustal template may be created (e.g., Brun et al., 2017 ; Buck, 1991 ; Coney, 1980 ; Osmundsen et al., 2005 ; Platt et al., 2015 ; Vanderhaeghe & Teyssier, 2001 ; Whitney et al., 2013). Since the classic paper by Block and Royden (1990), it seems widely accepted that MCCs form by viscous crustal flow as a mode of isostatic compensation in response to upper crustal thinning by extensional faulting. Block and Royden [1990] elegantly explain geophysical observations made around MCCs, suggesting that the flow of lower crustal material forms a dome, while the Moho remains flat. Yet, what is the actual mechanism of this

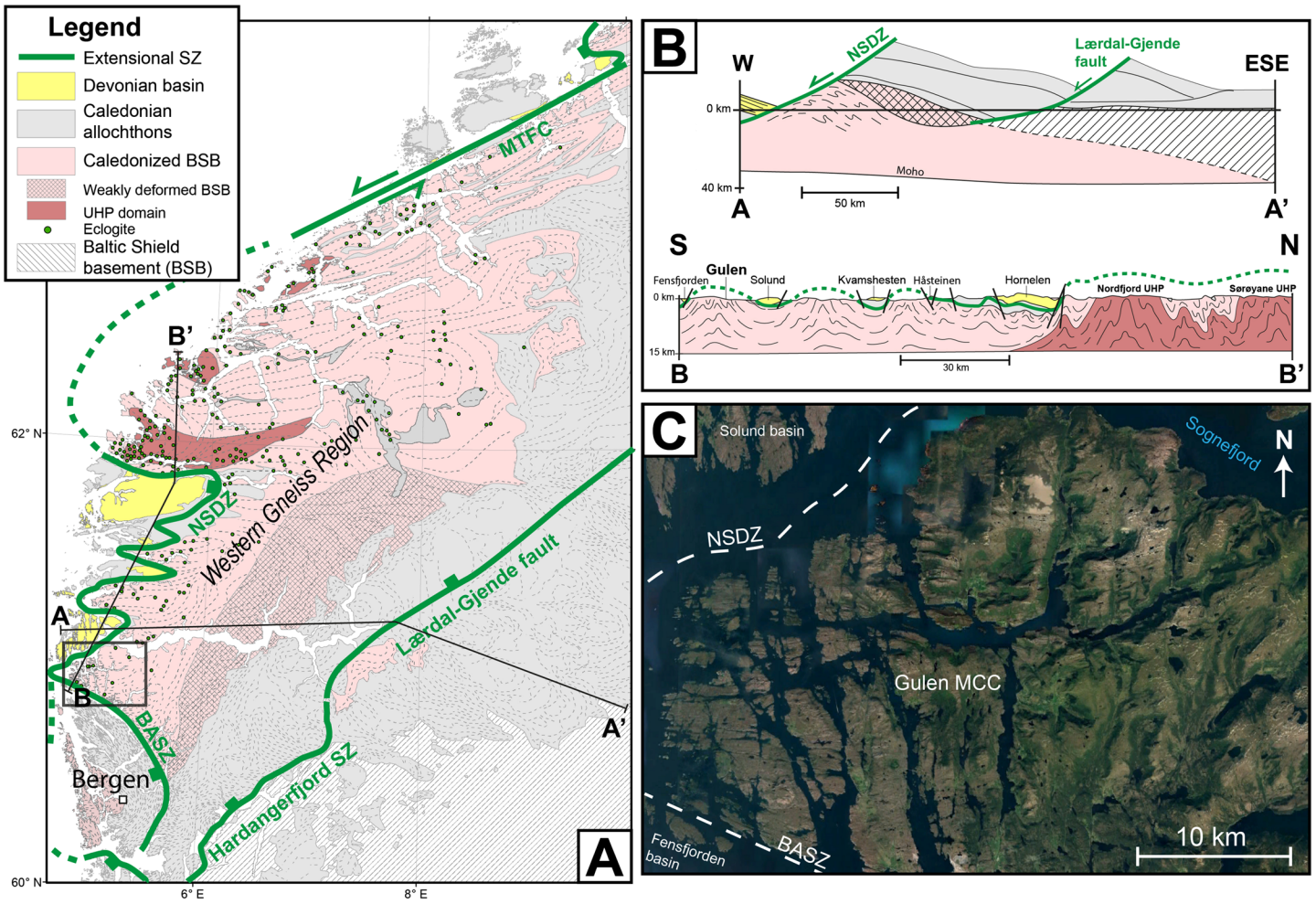

Figure 1. Overview of the study area. (a) Geologic map of the Western Gneiss Region. Ultrahigh-pressure domains after Hacker et al. (2010). Eclogite localities from Andersen et al. (1994), Krabbendam and Dewey (1998), Hacker et al. (2003), Hacker et al. (2010), and Hacker et al. (2015) and weakly deformed Baltic Shield basement (BSB) domain after Milnes et al. (1997). Structures of the extensional detachment system are shown in green. The location of cross sections in B is indicated, and the study area is marked by a rectangle. Abbreviations: BASZ = Bergen Arcs shear zone; MTFC = Møre-Trøndelag fault complex; NSDZ = Nordfjord-Sogn detachment zone. (b) Schematic cross sections of the WGR. A-A' redrawn from Milnes et al. (1997). B-B' based on Johnston, Hacker, and Ducea (2007b) and modified after Krabbendam and Dewey (1998), Braathen and Erambert (2014), this study and interpretation of regional structural data. (c) Satellite image of the Gulen MCC in between the Solund and Fensfjorden Devonian basins. Numerous islands in the western part of the area provide continuous and excellently exposed natural cross sections in E-W and N-S direction. Image from Google Earth.

flow that supposedly redistributes material within the deep crust? For hot lithospheres, it has been suggested that mid- to lower crustal channels of partially molten low-viscosity crust can form (e.g., Rey et al., 2009 ; Rey et al., 2011 ; Whitney et al., 2013). However, there are many examples of MCCs, including classical Cordilleran MCCs, where high-strain rocks are in solid state and no such channels are observed (e.g., Cooper et al., 2017; Platt et al., 2015). Further complexity arises if we consider MCCs as three-dimensional structures. In settings that involve a 3-D component of strain, like transtension, 3-D numerical experiments show extension-perpendicular flow of material (Le Pourhiet et al., 2012; Rey et al., 2017) instead of extension-parallel flow as it is commonly shown in schematic cross sections of MCCs. Therefore, we need detailed constraints on the internal architecture of deeply eroded MCCs that can help us to unravel the 3-D kinematics and mechanisms of postorogenic crustal flow.

The Western Gneiss Region (WGR) of the SW Scandinavian Caledonides (Figure 1) is an excellent place to do this. It represents the deeply eroded core of a Silurian continent-continent collision orogen where large parts of the crust were turned around during Devonian postorogenic transtension (e.g., Krabbendam & Dewey, 1998). Material metamorphosed in the orogenic root at high- or even ultrahigh-pressure

conditions was brought back to the surface in the time it took to deposit Devonian supradetachment basins (e.g., Eide et al., 2005; Templeton, 2015). The processes responsible for this crustal revolution are recorded in MCCs in the footwall of large-magnitude extensional detachments along the western coast of southern Norway (Figure 1b). The Gulen MCC, which is the southernmost of these structures, offers particular exposure conditions. Numerous islands with an orthogonal set of ideally oriented coastlines provide almost continuous high-quality exposures, which can be easily accessed by boat (Figure 1c). In this study, we provide a detailed look inside the anatomy of a particularly well-exposed postorogenic MCC in order to understand the viscous flow of the crust during transtension. We approach this issue from the micro- to the megascale to constrain the timing, quantity, and kinematics of ductile strain as well as the metamorphic conditions and deformation processes.

2. Geologic Setting

The WGR of southern Norway comprises Mesoproterozoic crust of the Baltic Shield that was subducted below Laurentia during Caledonian orogeny. The pre-Caledonian configuration of this part of the Baltic Shield was largely formed through the 1.2–0.9 Ga Sveconorwegian orogeny, involving widespread magmatism and migmatization (e.g., Bingen et al., 2005; Coint et al., 2015 ; Engvik et al., 2000 ; Kylander-Clark & Hacker, 2014 ; Røhr et al., 2004 ; Slagstad et al., 2018 ; Wiest et al., 2018).

NW-directed Caledonian subduction of the Baltican margin is reflected by increasing peak metamorphic conditions and deformation of Baltic Shield basement from SE to NW (e.g., Griffin & Brueckner, 1980; Hacker et al., 2010). Deep burial of the Baltican crust is witnessed by the widespread occurrence of high-pressure eclogites and externally derived mantle rocks, which have been inserted in the subducted continental crust from the overlying mantle wedge (e.g., Brueckner, 2018). Ultrahigh-pressure conditions are recorded in three distinct domains in the NW portion of the WGR (e.g., Cuthbert et al., 2000; Hacker et al., 2010 ; Root et al., 2005). Eclogite ages, which reflect subduction and peak metamorphism, range mostly from 430 to 395 Ma. They overlap in part with U-Pb zircon ages from granitic leucosomes (405–390 Ma; see compilation by Kylander-Clark & Hacker, 2014). Partial melting and local ultrahigh-temperature metamorphism occurred during high-temperature equilibration (e.g., Engvik et al., 2018; Ganzhorn et al., 2014; Gordon et al., 2013; Kylander-Clark & Hacker, 2014; Labrousse et al., 2011). Yet, it remains controversial to what extent melting initiated at ultrahigh-pressure conditions (e.g., Kohn et al., 2015) and whether pressure estimates reflect other processes than burial only (e.g., Vrijmoed et al., 2009). Amphibolite-facies reworking and exhumation of the WGR are dated by U-Pb monazite (410–390 Ma; Hacker et al., 2015; Holder et al., 2015), U-Pb titanite (405–385 Ma; Kylander-Clark et al., 2008; Spencer et al., 2013), U-Pb rutile (400–375 Ma; Butler et al., 2018; Cutts et al., 2019), and Ar-Ar white mica ages (405–375 Ma; Chauvet & Dallmeyer, 1992; Walsh et al., 2007; Young et al., 2011; Walsh et al., 2013). These ages show regional trends with younger ages toward the NW and imply progressive SE to NW unroofing of the WGR between 400 and 375 Ma.

Exhumation models of the WGR commonly involve two stages. The first stage is seen either as postorogenic eduction of the continental slab (Andersen et al., 1991; Fossen, 1992), gravity-driven ductile rebound of the orogenic root (Milnes et al., 1997; Milnes & Koyi, 2000), or flexural rebound and flattening of the slab (Cutts et al., 2019). A second phase comprising transtensional collapse of the overthickened crust and the formation of large-magnitude detachments is widely accepted (e.g., Butler et al., 2015; Fossen, 2010; Krabbendam & Dewey, 1998). Indeed, most structures in the WGR, from supradetachment basins to the ultrahigh-pressure domains, follow the trend of sinistral transtension (Dewey, 2002; Fossen et al., 2013; Krabbendam & Dewey, 1998; Osmundsen & Andersen, 2001). The felsic gneisses of the WGR were pervasively deformed during amphibolite-facies coaxial shear deformation with increasing intensity from E to W (Andersen et al., 1994; Hacker et al., 2010; Milnes et al., 1997). The gneisses are folded into tight, kilometer- to centimeter-scale, extension-parallel upright folds (Chauvet & Seranne, 1994). Large-magnitude, ductile-to-brittle detachments juxtapose the coaxially stretched, eclogite-bearing crust of the WGR with remnants of Caledonian allochthons and Devonian supradetachment basins (Andersen et al., 1994; Krabbendam & Dewey, 1998; Osmundsen & Andersen, 2001; Braathen et al., 2004; Johnston et al., 2007a; Johnston et al., 2007b).

The most important Devonian structure in SW Norway, the Nordfjord-Sogn detachment zone (NSDZ), is strongly undulating around E-W axes. Scoop-shaped Devonian basins occupy synformal positions, while

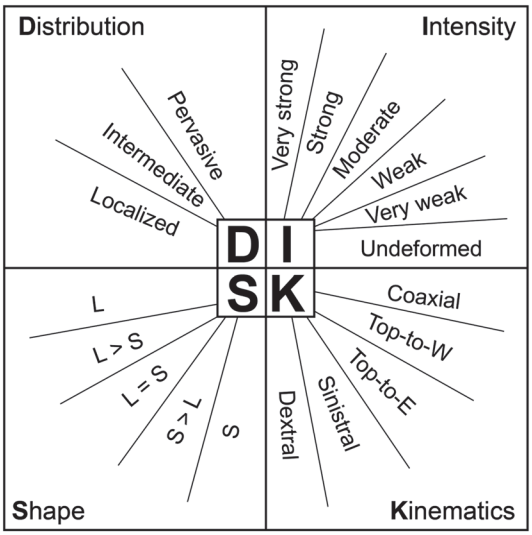

Figure 2. Schematic illustration of the DISK scheme for semiquantitative description of ductile deformation. The four parameters can be recorded as alphanumeric values, using mobile field mapping devices. See text for explanation of the parameters.

the WGR forms several E-W elongated culminations (antiforms) in the footwall of the undulating detachment. The portion of the WGR situated between the Møre-Trøndelag fault complex and the Hornelen basin (ca. 62° N, Figure 1a) can be seen as the largest culmination of the WGR. A magnitude smaller are the culminations in between the Devonian basins (Figure 1b). While the entire WGR can be seen as one giant MCC (Andersen & Jamtveit, 1990; Krabbendam & Dewey, 1998; McClay et al., 1986), we find it useful to apply the MCC concept (Brun et al., 2017; Platt et al., 2015; Whitney et al., 2013) also to the second-order antiformal culminations in the footwall of the NSDZ.

The Gulen MCC represents the southernmost culmination of the WGR and consists of strongly reworked Baltic Shield basement separated from overlying Devonian basins by the NSDZ and its southern continuation, the Bergen Arcs shear zone (BASZ; Wennberg et al., 1998). Precambrian protoliths were mainly formed during the 1.0 Ga Sveconorwegian orogeny as dated by U-Pb zircon ages of granitic leucosomes from migmatites (Wiest et al., 2019) and U-Pb zircon and monazite ages of local occurrences of granulite-facies rocks (Røhr et al., 2004). The area hosts the southernmost exposures of Caledonian eclogite in the Baltic Shield basement (Winsvold, 1996). Peak metamorphic conditions of the nearby Lavik eclogites have been constrained to 700°C, 2.3 GPa (Hacker et al., 2003). Previously published Ar-Ar ages group narrowly around 394 Ma (Boundy et al., 1996; Chauvet & Dallmeyer, 1992; Walsh et al., 2013), and Hacker et al. (2003) suggested rapid exhumation of the eclogite-bearing WGR along the southern segment of the NSDZ.

3. Semiquantitative Mapping of Ductile Strain

In order to reveal strain variations across a large area, we developed a scheme for the systematic description of ductile strain in outcrops, considering four main parameters: distribution, intensity, shape of the strain ellipsoid, and kinematics (Figure 2). The acronym DISK makes it easy to remember the parameters, which can be easily recorded in a numeric scheme for each visited locality. With the help of mobile mapping devices (e.g., Midland Valley Field Move Clino™), a large number of data points can be efficiently collected and exported to GIS software for data analysis and visualization.

The first parameter in the DISK scheme describes whether the deformation is localized, intermediate, or pervasive on the scale of 1–10 m. The intensity of the strain is recorded in five steps (very weak –very strong) plus an additional value for undeformed rocks. It should be noted that the intensity of the strain refers to the deformed portion of the outcrop, and hence, this parameter needs to be read together with the distribution parameter. For example, an outcrop with pervasive strong deformation records more bulk strain than an outcrop with localized strong deformation. The shape of the strain ellipsoid follows the common classification from L-tectonites to S-tectonites. Our classification includes coaxial deformation and noncoaxial deformation. Because shear sense indicators are sometimes ambiguous, this parameter can be furthermore improved by additionally recording the certainty of the observation with a second parameter (e.g., uncertain; certain; very certain).

3.1. Dataset Presentation

The collection of data presented in this study is prepared for use in GIS software and can be accessed online (https://doi.org/10.6084/m9.figshare.c.4697006.v1). Our field data comprise 36 eclogite localities, 1264 structural measurements, and 216 structural data that have been digitized from Winsvold (1996). Around 190 localities have been classified with the DISK scheme, and in addition we present more than 400 georeferenced and commented field photos. The trace of the foliation has been interpreted from structural measurements and high-resolution orthophotos. The same accounts for the boundaries of mapped units. Our field results are presented in a newly compiled geological map and accompanying cross sections (Figure 3). In addition, we present the results from DISK mapping in Figure 4 with symbols for each parameter overlaying the map.

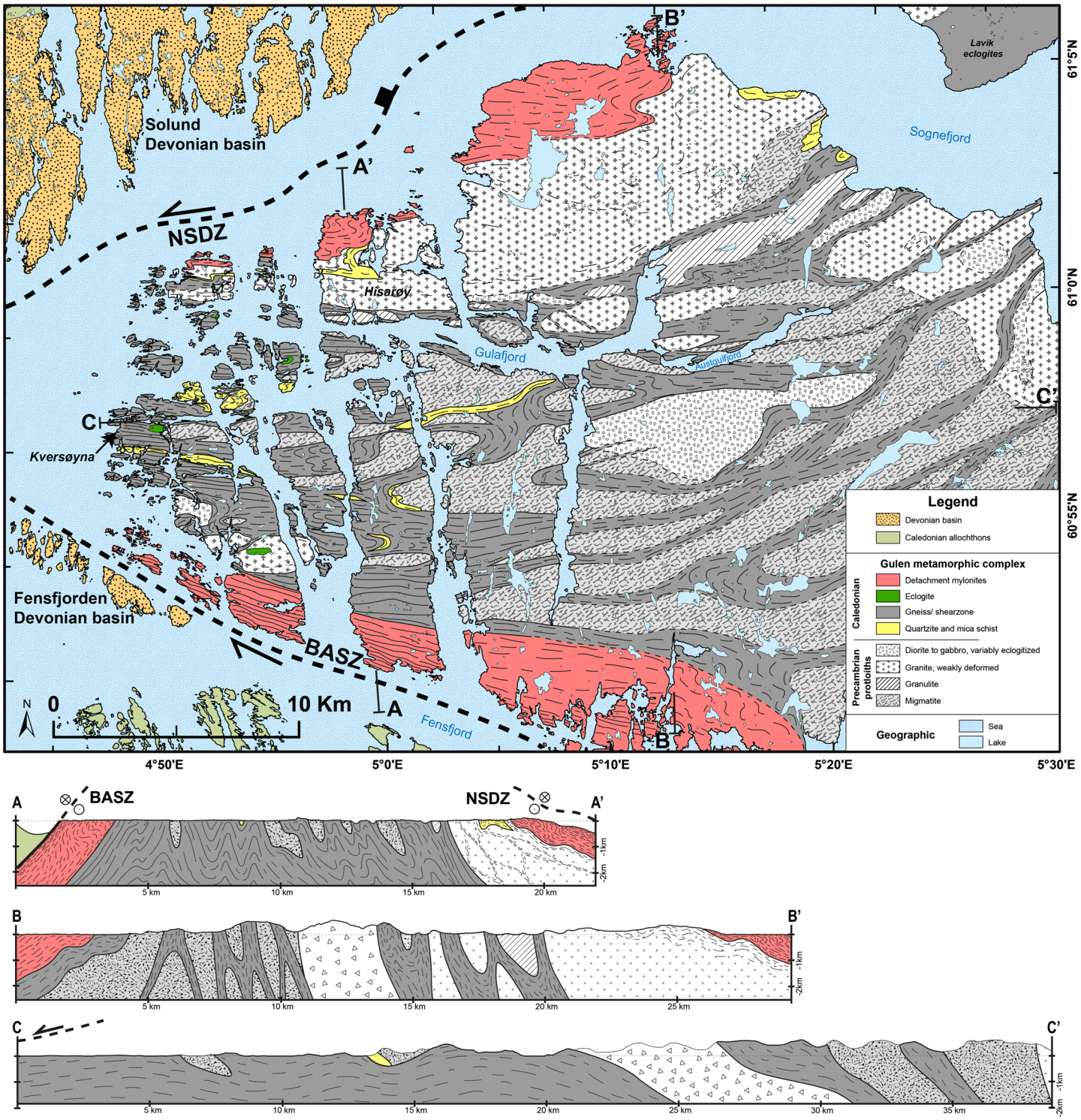

Figure 3. Newly compiled geologic map and cross sections of the Gulen area based on recent field mapping, Kildal (1970); Winsvold (1996); Ragnhildstveit and Helliksen (1997); Wennberg et al. (1998); Røhr et al. (2004). Abbreviations: BASZ = Bergen Arcs shear zone; NSDZ = Nordfjord-Sogn detachment zone.

4. Structural Architecture of the Gulen MCC

Our newly compiled geologic map and cross sections of the Gulen MCC are shown in Figure 3. The overarching structure of the MCC can be described as an open, south-verging antiform (Figure 3, cross

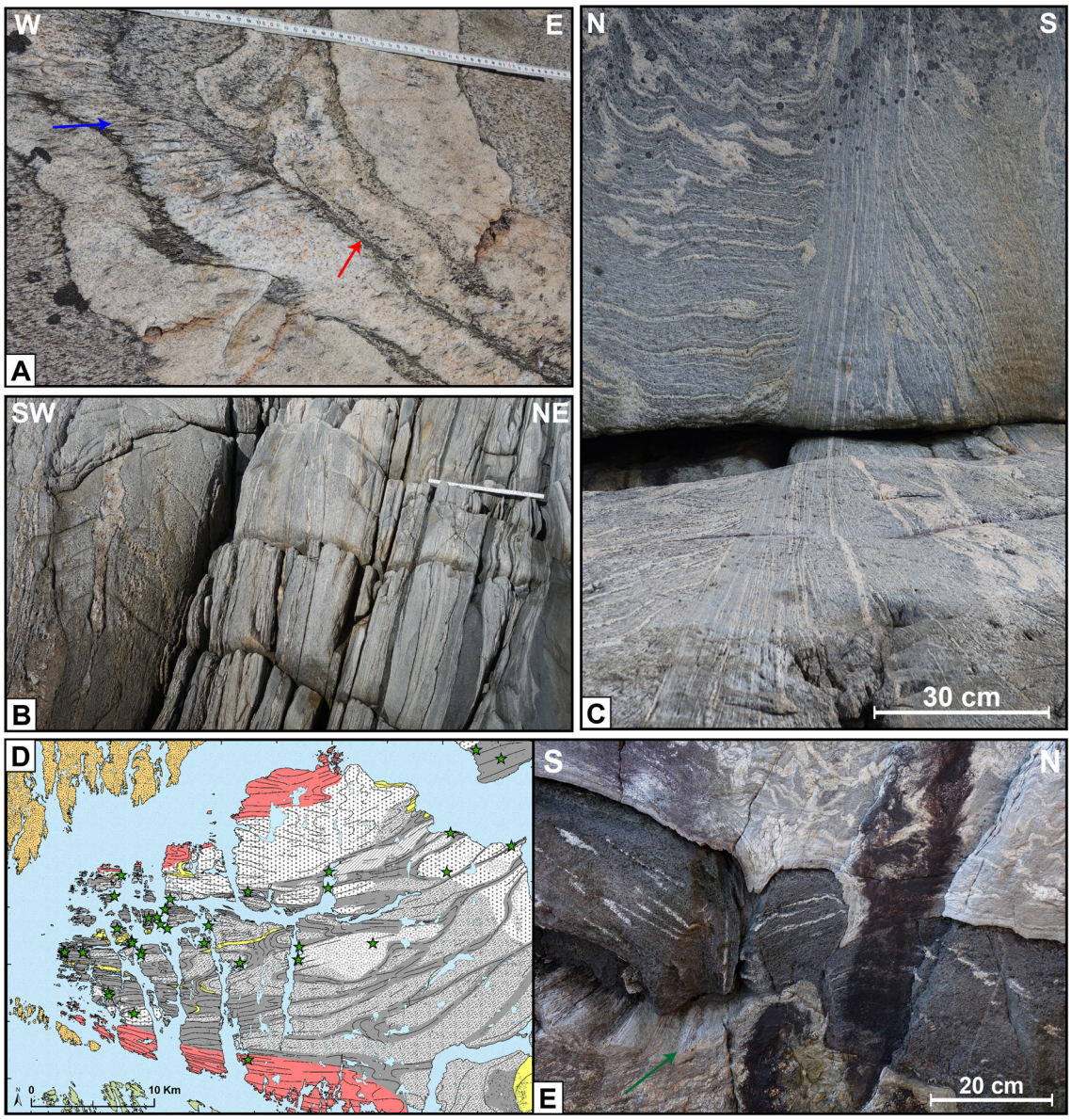

Figure 4. Distinguishing Precambrian protoliths from Caledonian shear zone rocks (a–c) and field occurrence of Caledonian eclogites (d and e). (a) Precambrian granodiorite intruded by granitic dykes. Weak Caledonian shear strain is localized at the dyke margins where they are preferentially oriented (red arrow). In case of less-suited orientations, the foliation transects the dyke (blue arrow). Ruler for scale. (b) Coarse-grained Precambrian migmatite (left side) is transformed into Caledonian banded gneiss in a meter-scale shear zone. The thin amphibolite layers represented originally mafic boudins in migmatite. Same locality as (a). Ruler is 40 cm. (c) Localized coaxial shear zone in Precambrian migmatite exposed in three dimensions. The straight trend and the sharp northern boundary may indicate that this shear zone has localized along a preexisting brittle feature. (d) The map of eclogite localities shows the highest concentration of eclogite bodies in the western core of the MCC. (e) Eclogitized mafic dyke in Precambrian migmatite. The dyke was boudinaged during migmatization, as boudin necks are filled with leucosomes. The protolith relationship was preserved because eclogitization was static and left the migmatite unchanged. However, eclogitization liberated fluids that were consumed by the host rock and led to garnet and white-mica growth in a narrow zone around the mafic body (green arrow). Note that minor shear deformation localized later at the hydrated contact zone.

section A) that plunges shallowly toward the west. The MCC is bound to the NW by the shallowly dipping NSDZ, which is overlain by the extensive Solund basin in the hanging wall. To the south, the MCC is bound by the steep northern BASZ. In contrast to the NSDZ, the hanging wall of the BASZ is occupied by large remnants of Caledonian allochthons of the Bergen Arcs and Devonian sediments are preserved only in an isolated fault-bounded block of the Fensfjorden basin. Bathymetric lineaments seem to indicate that the NSDZ and the BASZ merge offshore, just west of Figure 3, and form a well-defined western boundary of

the MCC. In contrast, there is no clear eastern boundary of the MCC, but rather a gradual transition into weaker deformed portions of the WGR (Figures 1a and 1b). This transition coincides with a rotation of structural trends from E-W in the MCC to NE-SW and the disappearance of eclogites toward the east. In E-W direction, the gneissic fabrics within the MCC appear shallowly undulating and rotate from generally easterly dip in the east to westerly dip in the west (Figure 3, cross section C). In three dimensions, thus, the shape of the Gulen MCC does not conform to a simple dome shape, but rather it must be described as a hyperbolic surface with marked N-S as well as E-W asymmetry.

Our mapping shows that the Gulen MCC comprises two fundamentally distinct structural units: first, mylonites that formed in relation to the extensional detachment system on the flanks of the MCC and, second, a high-grade metamorphic core. Low-grade retrogression overprinted higher-grade fabrics in the detachment mylonites. In contrast, the metamorphic core preserves amphibolite-facies fabrics, and low-grade retrogression is absent. The following sections will present detailed descriptions of how the crust was transforming inside this MCC.

4.1. How to Distinguish Precambrian Protoliths from Caledonian Shear Zones?

One of our main objectives was to quantify the amount of reworking of the Baltic Shield basement during the Caledonian orogeny. The distinctive feature of the Precambrian rocks is that they formed at high temperatures and involve large amounts of melt. Therefore, they are consistently coarse grained, which makes them easily discernible from rocks that experienced Caledonian solid-state shear deformation and associated grain size reduction (Figure 4). The oldest rocks are a metasedimentary sequence that has been intruded by a large gabbro and countless mafic dykes. The metasediments have been almost entirely migmatized, and only quartzites are preserved as relicts within the migmatites. Large granite plutons intruded in the northern half of the area. A distinct belt of coarse-grained gneissic rocks with granulite facies assemblages (Røhr et al., 2004) runs along the boundary of the largest of these plutons.

We find features that indicate a considerable time gap of cooling between Sveconorwegian migmatization and the initiation of solid-state shear deformation. In low-strain areas, shear deformation is commonly localized along primary lithological heterogeneities like dyke margins (Figure 4a) and probably preexisting brittle features (Figure 4c). With increasing strain, these shear zones grow in width and transform the coarse-grained Precambrian protoliths into medium-grained banded gneisses, where primary lithological relationships are obscured (Figure 4b).

4.2. Eclogites Record Processes in the Orogenic Root

Numerous eclogite localities (Figure 4d) demonstrate that the crust within the MCC represents parts of the former orogenic root. They occur dominantly in the core of the culmination, and the concentration of eclogite bodies and pods increases from E to W. The eclogites occur mostly as isolated lenses within felsic gneisses, as it is typical all throughout the WGR. In contrast to other portions of the WGR, however, eclogitization in the Gulen MCC appears to have been a static process. There are no eclogite-facies fabrics, but pre-eclogite textural relationships are preserved. Figure 4e shows a mafic dyke that has been boudinaged during Mesoproterozoic migmatization. Later, the mafic dyke has been entirely eclogitized, while the migmatite remained unaltered. However, there are several centimeter-thick zones around the eclogitized dyke where white mica and garnet overgrow the migmatite fabric. These observations suggest that the eclogitization of hydrous mafic rocks liberated fluids that were consumed by the immediate host rock leading to overgrowth of eclogite-facies minerals. Phengite-quartz veins, found in many eclogites, appear to be related to the same process. Almost all of the eclogites in the Gulen MCC were retrogressed to some extent. The relation between eclogite retrogression and deformation of felsic gneisses is explained in section 6 and discussed in section 7.1.

5. Caledonian Shear Strain

The width of gneissic shear zones ranges from the centimeter scale to the kilometer scale. The distribution of deformation at the mesoscale classified with the DISK scheme shows no systematic variations within the MCC (Figure 5). Localized mesoscale shear zones are restricted to low-strain domains, and most shear zones are tens of meters to kilometers wide. Therefore, variations in the distribution of shear zones become visible only at the map scale.

10.1029/2019TC005708

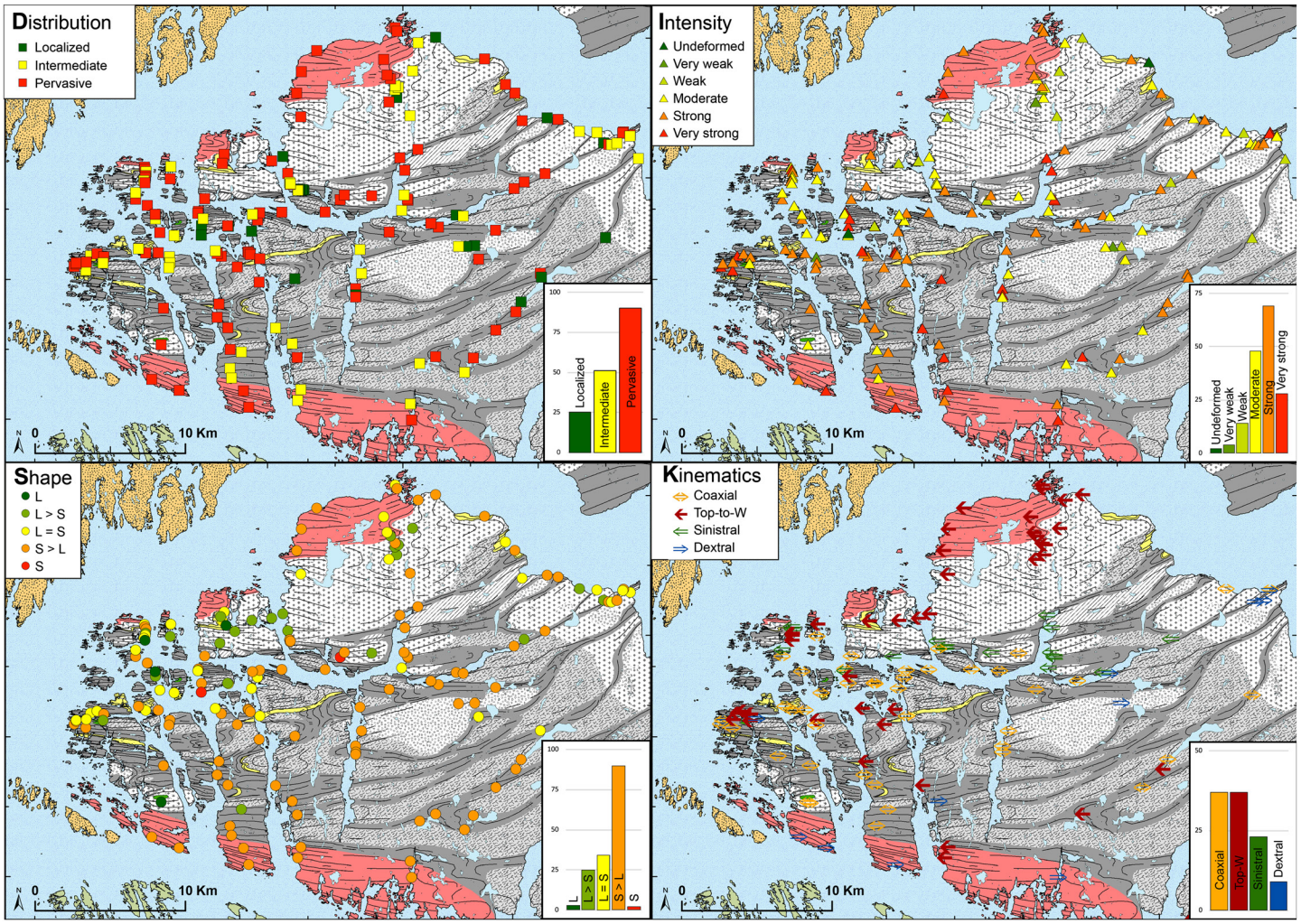

Figure 5. Results from DISK mapping: Each parameter is presented by symbols overlaying the geologic map and a histogram. Note that undeformed localities have usually not been recorded with the DISK scheme and, hence, are underrepresented.

In the eastern part of the area, shear deformation localized in an anastomosing network of discrete shear zones cutting through little deformed protoliths. Along the N-S cross section B (Figure 3), 45% of surface exposures are shear zone rocks, but within the core (excluding the detachment mylonites), only 25% of the protoliths have been significantly deformed. Toward the west, these isolated shear zones merge and form a coherent mass of highly sheared gneisses containing only isolated blocks of undeformed protolith. Along cross section A (Figure 3), >80% of the protoliths have been transformed into shear zone rocks, and this value increases even further toward the west.

The mesoscale classification of strain intensity, shape of the strain ellipsoid, and kinematics shows systematic variations that distinguish the detachment mylonites from the core (Figure 5). The detachment mylonites are dominated by noncoaxial top-W fabrics with a dominant S > L shape and strong deformation intensity. Strain intensity is generally increasing toward the top of the detachment. Large areas below the NSDZ mylonites are occupied by granite plutons with weak to moderate strain and a dominant L > S fabric.

Further away from the detachments, in the core of the culmination, the deformation intensity increases again and coaxial S > L fabrics dominate in strongly deformed domains. Strain intensity is mostly classified as strong, while very strong deformation is only found where rheological contrasts create particular conditions for strain localization (e.g., large eclogites contained in gneiss). Weakly deformed domains in the core show a dominant L-shape of the coaxial background strain. In general, stronger shearing appears to be

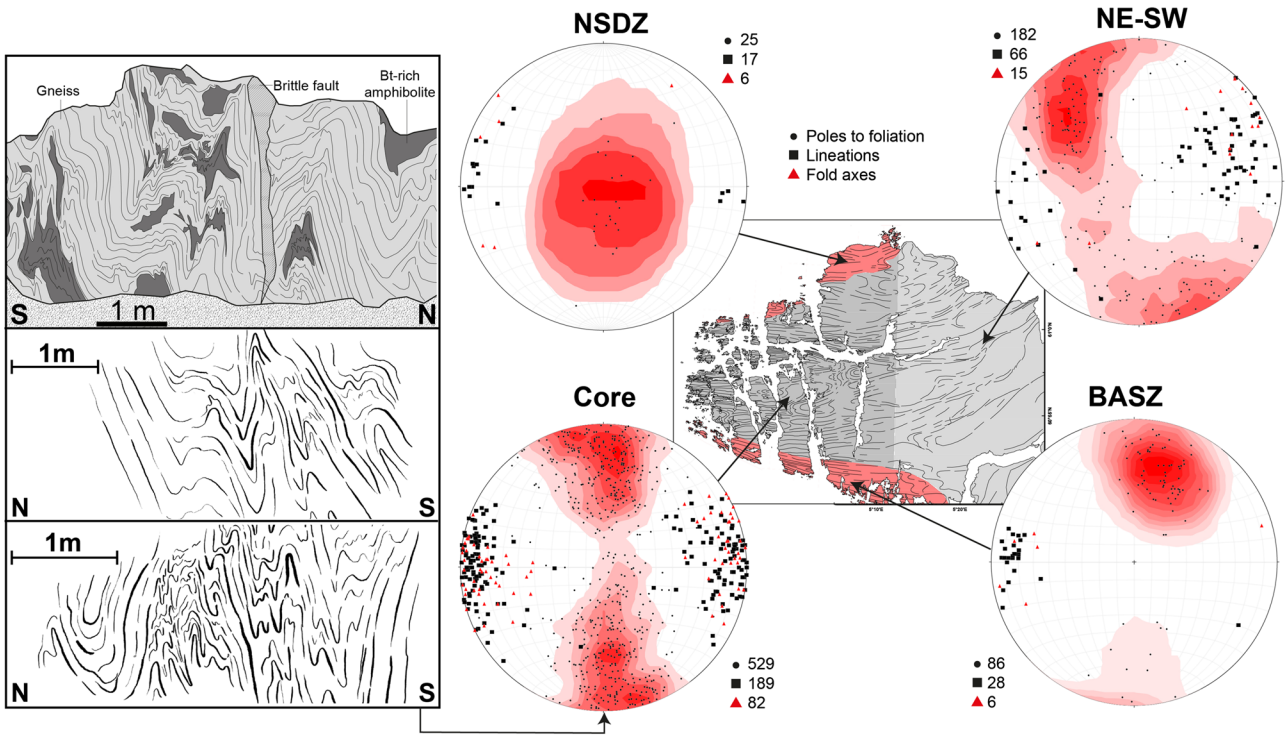

Figure 6. Lower hemisphere equal-area plots of structural data. Contours are plotted for poles to foliations. Four structural domains have been distinguished based on variations in fabric orientation. The inlet shows upright folds in gneisses of the core domain, redrawn from field photos. Most folds are tight to isoclinal. Multilayer buckling with small-scale parasitic folds occurs mostly in and around biotite-rich mafic layers.

associated with more planar fabrics, or in other words, the amount of E-W stretching correlates with N-S shortening. Noncoaxial fabrics occur to some extent also in the core of the MCC. They reflect overall top-to-W shearing by sinistral and dextral fabrics at the northward- and southward-dipping flanks of the culmination, respectively.

5.1. Fabric Orientations and Folding

Across the entire MCC, we find subhorizontal to moderately plunging lineations, lineation-parallel fold axes, and a corresponding girdle of foliations (Figure 6). For structural analysis, we distinguished four domains with distinct fabric orientations. Mylonites belonging to the NDSZ show WNW-plunging lineations and subhorizontal foliations. Mylonitic foliations are folded around NE-SW as well as NW-SE trending tight recumbent folds, consistent with vertical shortening. The mylonites of the BASZ show consistently WNW-plunging lineations and steeply SSW-dipping foliations. The mylonitic foliation is folded around isoclinal folds with SW-dipping axial planes that are parallel to the foliation. Lineations and fold axes in the core follow an E-W trend and plunge shallowly toward the east and the west. Foliations are mostly steep to subvertical and folded around E-W trending tight to isoclinal upright folds (Figure 6). These folds are observed from the outcrop scale to the map scale (compare Figure 3) and involve passive folding as well as active multilayer buckling. Fold tightness appears to be correlated to strain intensity, and fold amplitude seems to relate to shear zone width. However, it should be noted that even in an almost continuously exposed area like the one studied, the exact amplitude of such steep folds is practically impossible to constrain. Our cross section reconstruction implies amplitudes up to several kilometers in the most strongly deformed domain in the west of the MCC. It is also impossible to quantify the amount of E-W extension and N-S shortening in these kinds of rocks, but conservative estimates imply at least 70% of N-S shortening by upright folding in individual outcrops of strongly deformed gneisses.Toward the east, fabrics rotate into an orogen-parallel trend: lineations plunge mostly toward the NE and foliations dip mostly steeply toward the SE. Besides this change in orientation, the NE-SW-oriented shear zones show the same characteristics as the shear zones in the core domain.

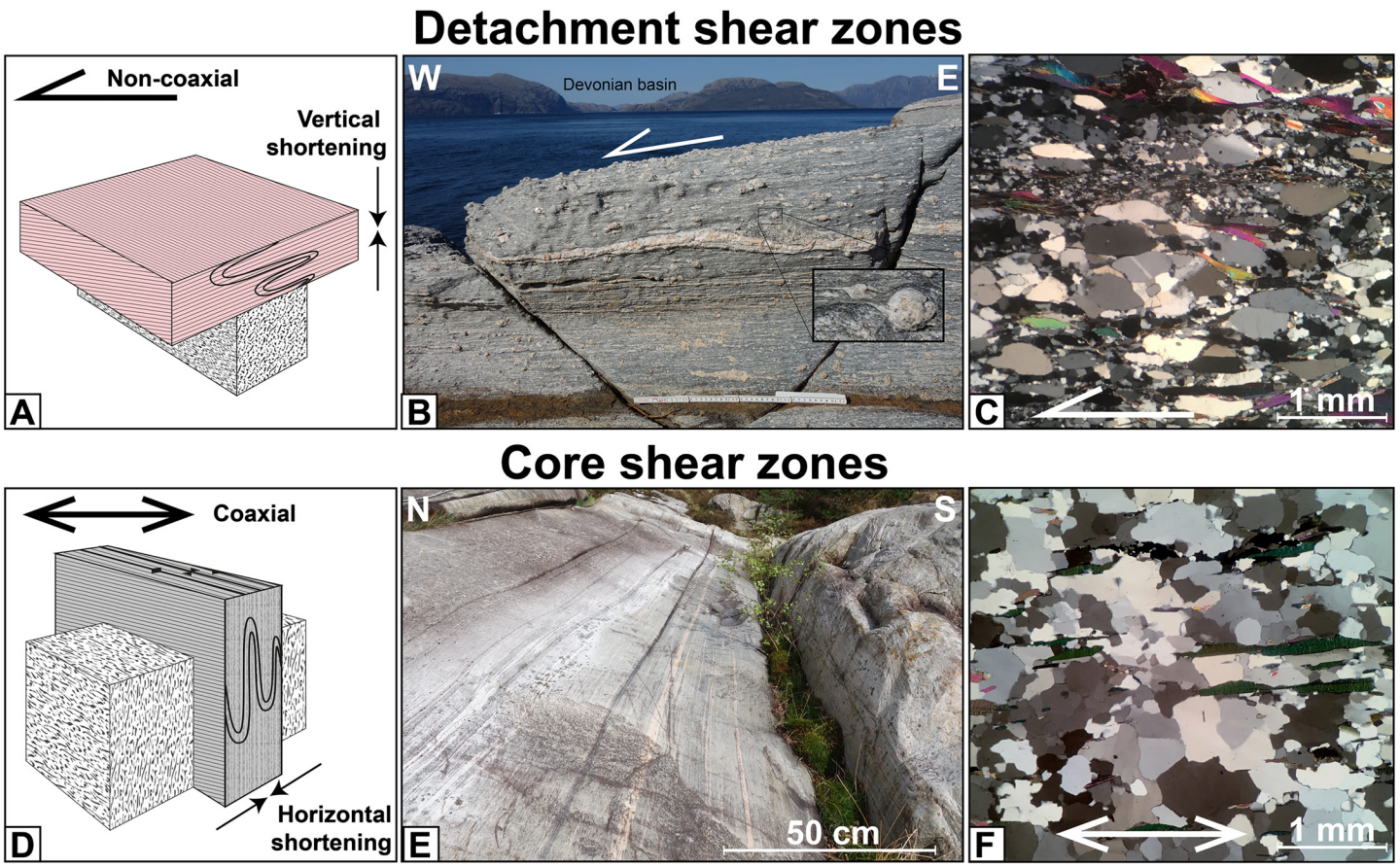

Figure 7. Two endmembers of shear zones developed in the detachment zone (a–c) and the core (d–f). (a) Schematic sketch of subhorizontal detachment shear zone with underlying constrictional domain. (b) Outcrop photo of typical rock in the detachment mylonites. This granitic mylonite contains large feldspar σ- and δ-porphyroclasts within a fine-grained phyllonitic matrix that indicate top-to-W noncoaxial deformation (see inlet). Contrasting rheological behavior of feldspar and the quartz-rich matrix, respectively, indicate lower greenschist facies deformation. The cliffs in the background on the other side of the Sognefjord are part of the Solund Devonian basin. (c) Photomicrograph (cross-polarized light) of quartzite from the detachment mylonites with a composite microstructure. Large grains showing grain boundary migration microstructures and indicate high-temperature low-stress recrystallization (Regime 3, Platt et al., 2015). The coarse-grained fabric is overprinted by fine-grained low-temperature, high-stress (Regimes 1–2) micro shear zones with bulging and subgrain rotation recrystallization. Both fabrics show asymmetry related to top-to-W shearing. (d) Schematic sketch of vertical and coaxial core shear zone, involving simultaneous N-S shortening and E-W extension. (e) Outcrop photo of a typical core shear zone. The mylonitic foliation is subvertical, fabrics are coaxial, and alternating feldspar- and quartz-rich layers show identical rheological behavior, indicative of high-temperature deformation. (f) Photomicrograph (cross-polarized light) of quartzite from a core shear zone with a simple microstructure of coarse-grained quartz. Grain boundary migration microstructures are observed, but most grains are strain-free and abundant 120° triple junctions indicate high-temperature recovery. The absence of a clear shape or crystallographic preferred orientation in quartz and parallel mica grains indicates coaxial deformation.

5.2. Shear Zone Endmembers: Detachment vs. Core Shear Zones

Systematic variations in fabric orientation, ductile strain characteristics, as well as distinct metamorphic evolutions suggest that the detachment mylonites of the NSDZ and the shear zones in the core represent endmembers of shear zones that formed at different structural levels of the MCC (Figure 7). The BASZ seems to be an intermediate case.

5.2.1. Endmember 1: Detachment Mylonites of the NSDZ

In the detachment mylonites, which belong to the NSDZ, foliations are shallowly dipping to subhorizontal, and folds have subhorizontal axial planes (Figure 7a). Most fabrics are noncoaxial and consistently show top-to-W transport (Figure 7b). Another striking characteristic of the detachment mylonites is their record of progressive retrograde deformation from high-grade to low-grade conditions. Amphibolite-facies fabrics are partly preserved as relicts and comprise coarse grain boundary migration fabrics in quartz-rich lithologies, which indicate high temperatures and low flow stresses (Regime 3 microstructures, Platt et al., 2015). Yet, most samples show complex microstructures with greenschist-facies fabrics overprinting higher-grade

fabrics (Figure 7c). Subgrain rotation and bulging recrystallization of quartz to very fine grain sizes indicate high flow stress and low-temperature deformation conditions (Regime 1–2 microstructures). Progressive retrograde deformation appears to lead to increasing strain localization that is strongly related to fluid-rock interaction. There are large tracts of phyllonitic shear zones, both in mafic and felsic lithologies, and chloritization, saussuritization, and epidotization are abundant. Embrittlement of feldspar-rich layers is recorded by greenschist-facies quartz veins. Layers of amorphous greenish cataclasites, with thicknesses up to several meters, are parallel to the shallow-dipping foliation and indicate a progressive fault rock evolution from ductile to brittle conditions.

5.2.2. Endmember 2: Core Shear Zones

Shear zones in the core of the MCC have distinct structures and record a different metamorphic evolution. Foliations are steep to vertical and folded into tight to isoclinal upright folds. Subhorizontal lineations and mostly coaxial fabrics indicate overall pure shear deformation with simultaneous E-W stretching and N-S shortening (Figure 7d). Core shear zones preserve amphibolite-facies fabrics without further retrogression. In quartz-rich lithologies, these commonly involve grain boundary migration recrystallization of quartz at high temperatures and low flow stresses resulting in large grain sizes (Regime 3 microstructures, Figure 7 f). Feldspar layers in the gneisses are behaving entirely viscously and show identical rheological behavior as quartz-dominated layers (Figure 7e). Even though the core shear zones do not show evidence for low-grade fluid-related retrogression, there is clear evidence that they represented important fluid conduits at amphibolite-facies conditions. Fractures occur at sites of rheological heterogeneity, commonly related to extension-parallel folding, and are mineralized as quartz-feldspar veins. The importance of fluids during amphibolite-facies deformation is furthermore recorded by the relationship between shearing and eclogite retrogression, which is presented in section 6.

5.2.3. The Intermediate Case: The BASZ

The detachment mylonites of the BASZ show noncoaxial deformation and a similar metamorphic fabric evolution to the ones from the NSDZ, with low-grade retrogression overprinting higher-grade fabrics. Yet, there are some important differences between these two segments of the detachment system.

The northern BASZ represents an oblique dextral strike-slip segment of the detachment system (Wennberg et al., 1998) and along the southern boundary of the Gulen MCC, the shear zone dips consistently with ca. 60° toward SSW. Large domains of weakly deformed rocks, as found below the NSDZ, are absent in the footwall of the BASZ. In contrast, the BASZ mylonites show a gradual transition into core shear zones, and their fabric orientation is more similar to those observed in the core than those in the NSDZ. Folds in the BASZ indicate N-S shortening and do not show vertical shortening like the NSDZ mylonites. No remnants of the Caledonian nappe pile are exposed in between the Fensfjorden basin and the BASZ mylonites, and the Devonian sediments appear directly juxtaposed to the eclogite bearing crust. These observations suggest that the amount of excision and incision was larger along the southern bounding fault of the Gulen MCC than along its northern boundary. Incision of the strike-slip segment of the detachment has allowed parts of the high-grade core to become overprinted by retrograde strike-slip shearing along the BASZ. Yet, the same may account for the westernmost part of the NSDZ mylonites that contain retrogressed eclogites (Figure 4d).

6. Amphibolite-Facies Reworking of the Exhuming Crust

Pristine eclogites are preserved only in undeformed protolith domains (e.g., Figure 4e). Most eclogites were variably retrogressed at amphibolite-facies conditions. Larger eclogites within shear zones show progressive retrogression from the rim, with amphibolitized margins and eclogite in the core. The state of retrogression appears to be related to the position of the eclogites with respect to shear zones, the availability of fluids, and the size of the eclogite body. A particularly well-exposed locality on Kversøyna at the western apex of the MCC (see Figure 3 for location) shows that eclogite retrogression was fluid induced and simultaneous with shearing and folding of felsic gneisses.

6.1. Structure of the Kversøyna Locality

The 200-m-long and 100 m-wide coastal section (Figure 8) exposes strongly pervasively sheared gneisses and eclogite bodies of variable size, ranging from few meters to >100 m. The gneisses are folded around E-W trending fold axes into tight to isoclinal upright folds with undulating hinge lines. The eclogite bodies are boudinaged, indicating E-W stretching, and occupy synformal positions within the folded gneisses. A

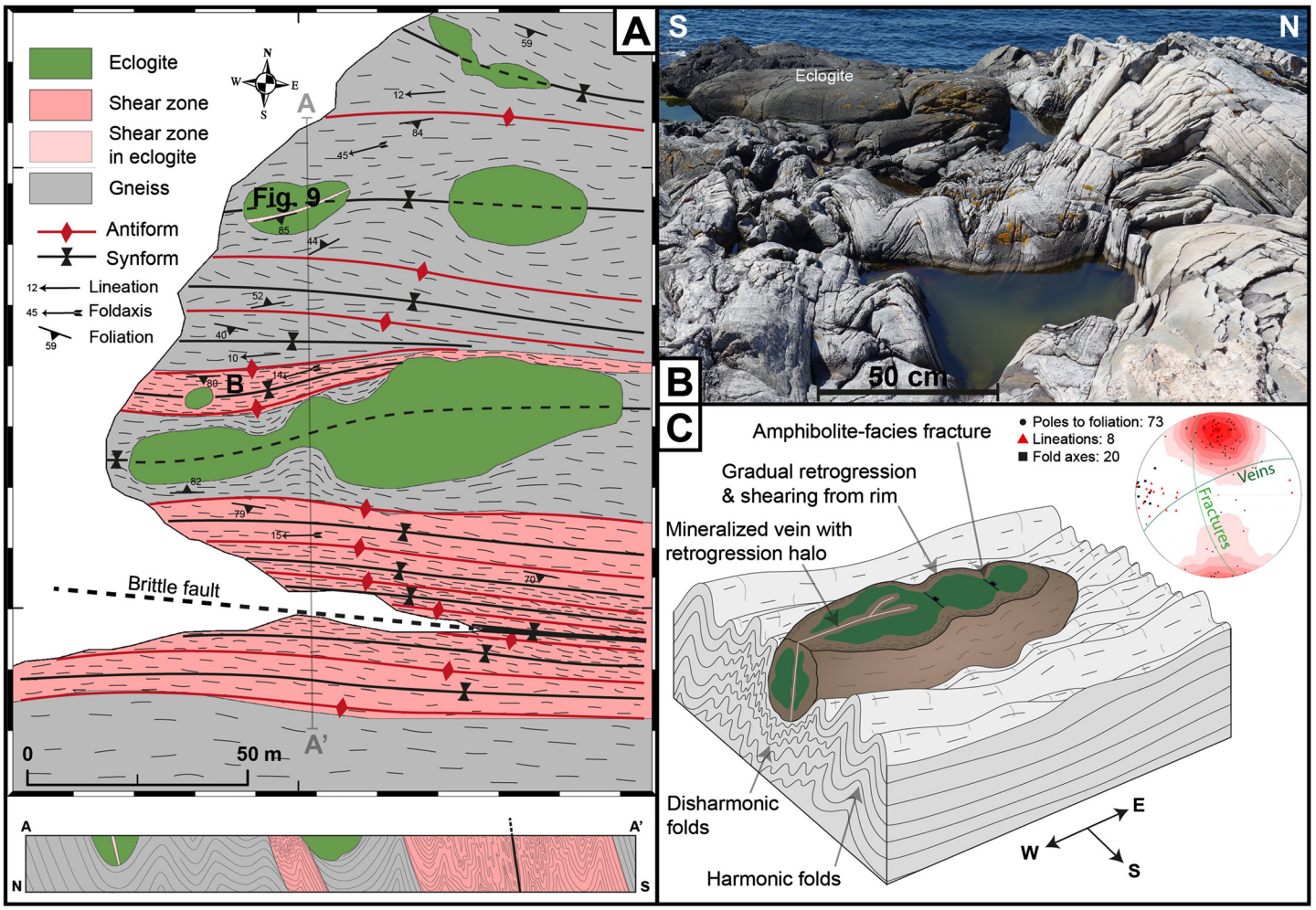

Figure 8. Overview of the Kversøyna locality (location marked on Figure 2). (a) Map and N-S cross section of the locality. Note the influence of dense and rigid eclogite lenses on the gneiss fabric and how fold tightness increases in high-strain zones. The strong fabric anisotropy in the larger shear zone has been exploited by a brittle fault, which is also marked in the coastline. (b) Outcrop photo of eclogite boudin in strongly folded gneiss. Location is marked in (a). (c) Schematic sketch illustrating the observed relationship between folding of gneiss and eclogite retrogression. The lower area equal-area plot shows structural data of the gneisses together with the mean orientation of amphibolite-facies fractures and mineralized veins in eclogite lenses.

weakly pronounced structural asymmetry could indicate a minor component of dextral simple shear, but the gneissic fabrics are symmetric and imply dominant coaxial deformation with synchronous E-W stretching and N-S shortening, like in the rest of the core domain. High-strain zones formed at the borders of the largest eclogite body and show a marked increase of fold tightness compared to the surrounding gneisses. The folded gneisses wrap around the eclogite lenses (Figures 8b and 8c). The folds in the gneisses are generally harmonic; however, in proximity to the eclogites, they get increasingly disharmonic (Figure 8c). The synformal positions of the eclogites within the gneisses, their boudinage, and their influence on folding as well as shear zone localization indicate that the eclogites formed rigid and dense anomalies that were perturbing the else homogeneous flow of the felsic gneisses.

6.2. Fluid-Induced Eclogite Retrogression and Rheological Weakening

Even though the eclogite lenses appear as homogeneous rigid blocks at first sight, a closer look reveals that their rheological behavior has been highly variable depending on their state of retrogression. The typical pattern of eclogite retrogression is a reaction front that moved from the rim of the body toward the core (Figure 8c). Retrogressed amphibolite margins have been sheared progressively together with the surrounding gneisses and indicate that rheological weakening accompanied retrogression.

The rheological contrast within the partially retrogressed mafic bodies leads to fracturing and boudinage of the eclogite domains (Figure 8c). Two conjugated sets of subvertical fractures strike roughly parallel and perpendicular to the maximum stretching direction, respectively. The extension-parallel set of fractures is mineralized with amphibole, plagioclase, and quartz (marked as veins in Figure 8c). In a large (> 20 m) eclogite, these veins are surrounded by decimeter-wide fluid alteration haloes. Within these fluid alteration zones, the eclogite has been retrogressed to undeformed amphibolite (Figure 9a). These mineralized fractures apparently represent corridors where fluids could enter the core of the eclogite and trigger retrogression, while dry domains of pristine eclogite, only centimeters apart, survived metastably until final exhumation.

On the microscale, retrogression is most advanced within fractures, where fluids have entered the rock (Figures 9b and 9c). From these fractures, the retrogression front spreads through the rock along microfractures and grain boundaries (Figure 9d). Microfractures and grain boundaries in omphacite show successive generations of symplectites with coarser symplectites in the core and finer symplectites at the rim. In some cases, symplectites are cut by fractures themselves and then replaced by amphibole (Figure 9c).

Like the retrogression at the rim of the eclogite bodies, retrogression in the core of the mafic lenses gives evidence for significant rheological weakening. The widest retrogression zone, measuring roughly 1 m in thickness, has been entirely transformed into an amphibolite-facies shear zone that cuts through the center of a large eclogite body (Figure 9a). Within this shear zone, not a single relict of the eclogite assemblage is preserved. The shear zone is cut itself by a mineralized fracture, giving evidence for brittle-ductile deformation cycles at amphibolite-facies conditions, probably caused by large rheological heterogeneity within the mafic body. This behavior is furthermore recorded by pseudotachylite formation in partially retrogressed and sheared domains of the eclogite.

Our observations show that the eclogite-bearing crust from the orogenic root was largely reworked at amphibolite-facies conditions. Shear zones appear to have served as conduits for amphibolite-facies fluids that entered undeformed domains through fractures. The availability of fluids clearly controlled the retrogression of eclogites and thereby rheological weakening that enabled viscous flow. These observations strongly resemble the processes observed in the famous Bergen Arcs eclogites (e.g., Austrheim et al., 1997), however, with the difference that they apply to retrogression and not during eclogitization.

7. Discussion: Crustal Flow Within the Gulen MCC

7.1. Eclogites as Time Markers of Postorogenic Viscous Flow

Eclogites within the Gulen MCC are robust time markers for processes that took place in the orogenic root as well as those associated with exhumation. Static eclogitization and the absence of eclogite-facies deformation fabrics indicate that the crust in the southernmost part of the Caledonian eclogite province was still relatively cold and rigid and did not deform pervasively during peak metamorphism. This is quite different from other parts of the WGR where eclogite-facies fabrics are well developed, probably because the crust was buried deeper and higher metamorphic grades were reached (e.g., Andersen et al., 1994; Braathen & Erambert, 2014).

In the Gulen MCC, extensive ductile deformation localized into shear zones and in broad zones of pervasive viscous flow. We find a consistent relationship pattern of eclogites being retrogressed in shear zones, while eclogites in undeformed domains remain mostly preserved. This indicates that the shear zones formed during the transtensional collapse of the overthickened crust (Mode II extension by Fossen, 1992) and after exhumation from eclogite facies conditions, possibly through eduction (Mode I extension). Obviously, we cannot exclude the possibility that some of the shear deformation may have occurred at an earlier stage. However, fabrics show a consistent orientation from the top of the detachment to the lowermost exposed parts of the metamorphic core. The rotation of fabrics from E-W into a more orogen-parallel trend toward the East represents an exception from the rule. Yet, shear zones in this domain show a metamorphic evolution similar to that in the rest of the core, the same relation between linear and planar fabrics and, most importantly, they also contain retrogressed eclogites. Hence, the NE-SW trending shear zones are likely to be postorogenic as well, and their orientation might relate to local orogen-parallel flow during unloading of the orogen (Duclaux et al., 2007). Our interpretation of postorogenic viscous flow in the Gulen MCC is supported by available thermochronological data (Boundy et al., 1996; Chauvet & Dallmeyer, 1992; Walsh

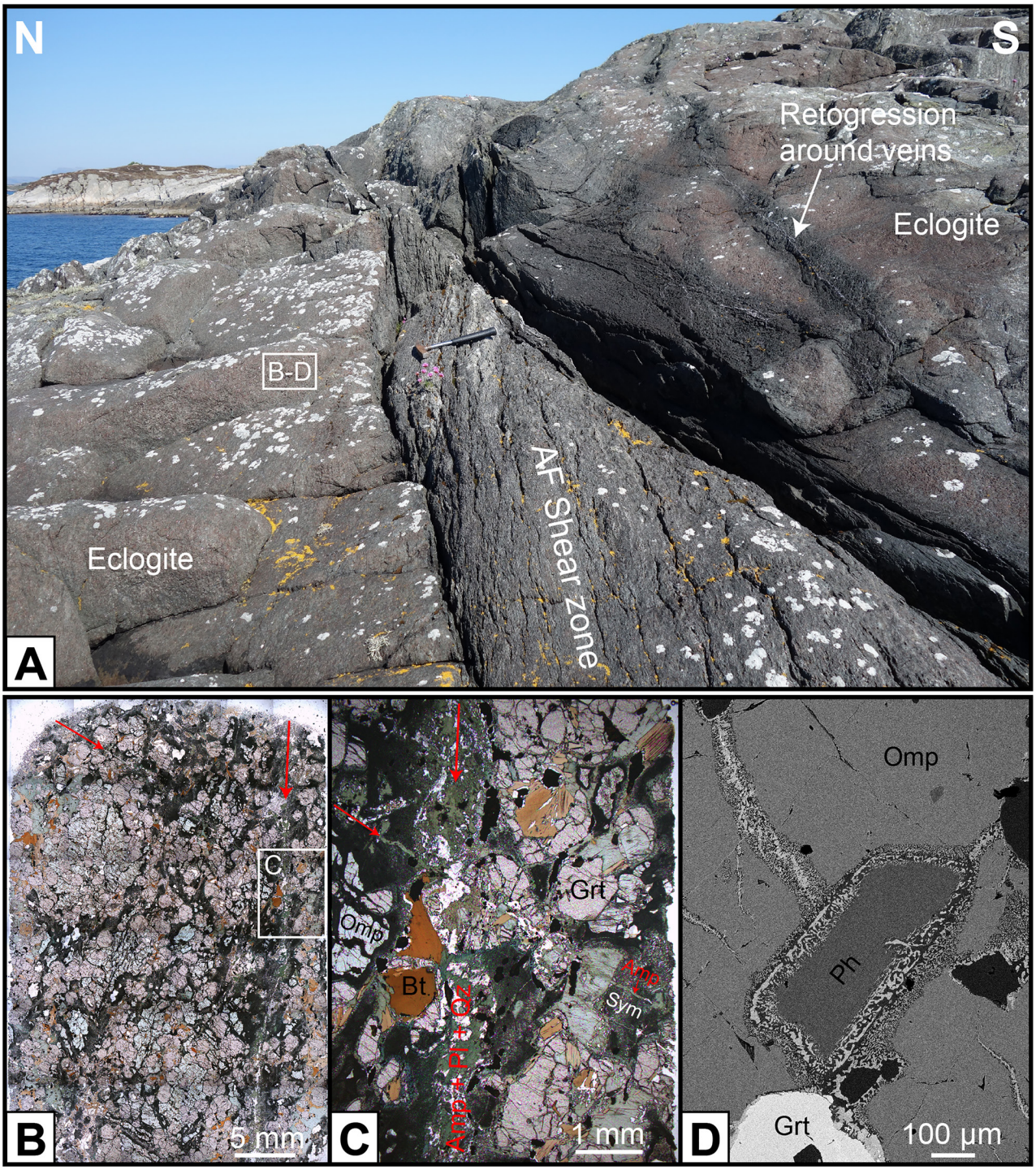

Figure 9. Fluid-induced eclogite retrogression from mesoscale to microscale. (a) Outcrop photo of fluid-induced retrogression in large eclogite body. Location is indicated in Figure 8a. Around mineralized veins, eclogite (red-green) was retrogressed statically to amphibolite (dark green to black). The largest retrogression zone in the center of the photo developed into an amphibolite-facies shear zone, which is cut again by a mineralized brittle fracture. Hammer for scale. (b) Thin section photomosaic (cross-polarized light) of partially retrogressed eclogite. Retrogression domains are easily recognized by the dark color of nontransparent symplectites and green amphiboles in contrast to the light-colored eclogite facies minerals. Retrogression is most advanced along a conjugate set of fractures (red arrows). Note how the retrogression front follows grain boundaries. (c) Close-up of the intersection of the mineralized fractures (red arrows). The larger fracture displays an amphibolite-facies mineralogy. Omphacite is surrounded by a rim of fine grained symplectites, which become coarser further away from the grain boundary and show progressive symplectite growth. Note how symplectites are transformed into amphibole, where they are cut by the small fracture. This relationship clearly demonstrates that even on the microscale, retrogression is a function of fluid availability. (d) Scanning electron microscope image of the least retrogressed eclogite domain. Retrogression advances along fractures and grain boundaries and leads to growth of submicrometer size symplectites.

et al., 2013) and interpretations of previous works in the surrounding areas (Andersen et al., 1994; Hacker et al., 2003; Milnes et al., 1997).

7.2. Viscous Flow at Distinct Structural Levels: Kinematically Linked, Mechanically Decoupled

Our results from the Gulen MCC fit very well within the general framework of postorogenic exhumation of the WGR by shearing along the NSDZ during sinistral transtension (e.g., Krabbendam & Dewey, 1998). Yet, our results are not fully explained neither by simple shear detachment models (e.g., Hacker et al., 2003; Souche et al., 2013), nor by homogeneous constriction as predicted from transtension (e.g., Dewey, 2002; Fossen et al., 2013; Krabbendam & Dewey, 1998), nor by simple vertical thinning of the overthickened crust (e.g., Andersen et al., 1994). All of these elements need to be integrated in a dynamic model of detachment and footwall evolution, to explain the distinct deformation that we observe at various levels of the extending crust.

At the presently exposed level, crustal flow within the Gulen MCC is entirely solid state. The crust appears to represent a coherently stretched block with significant strain variations in three dimensions (Figure 10). We find distinct structural levels that appear kinematically linked while mechanically decoupled. They formed within the same kinematic boundary conditions of sinistral transtension but represent different metamorphic conditions and hence different rheologies. On top, the detachment level shows simple shear with vertical thinning and the characteristic overprint of greenschist facies and semibrittle fabrics on higher-grade fabrics. In contrast, the lowest level shows pervasive coaxial amphibolite-facies viscous flow of the crust reaching extreme amounts of simultaneous E-W stretching and N-S shortening. A key finding of this study is that the coaxial high-grade fabrics in the core experienced no further low-grade overprint. As such, it must represent a structural level that is distinct from the noncoaxial detachment zone with its consistent retrograde overprinting relationships. In between these two levels, we find minor remnants of an intermediate domain of localized amphibolite-facies deformation, which involves constriction and minor vertical thinning. These distinct amphibolite-facies domains resemble the localized-distributed transition within the viscous crust postulated by Cooper et al. (2017). Today, we find all these different structural levels along the same exposure level as observed along cross section A (Figure 3). Their systematic variations in metamorphic conditions and strain characteristics imply, however, that they formed at different vertical levels of the crust and were later juxtaposed during core-complex exhumation.

7.3. Inward Flow Through Differential Folding ("Stockwerk Folding")

The N-S cross sections through the WGR and the Gulen MCC show intensive extension-parallel folding (compare Figure 1B and Figure 3) in contrast to shallowly undulating, parallel fabrics seen in E-W sections. According to our mapping in the Gulen MCC and the interpretation of large-scale fold patterns along the west coast of the WGR (Figure 1B), different crustal levels experienced apparently different amounts of N-S shortening. The detachment zone and the overlying basins show mostly open folds, although thrusts and reverse faults within the basins record locally larger amounts of syn-sedimentary N-S shortening (Osmundsen et al., 2019). The WGR footwall, however, is pervasively folded into tight to isoclinal upright folds from the scale of meters to tens of kilometers. Thus, the amount of N-S shortening in the footwall of the NSDZ appears to be significantly larger than in the overlying nappes and the detachment zone itself (Braathen & Erambert, 2014). These extension-parallel folds have been related to a distinct tectonic phase of regional N-S compression (e.g., Chauvet & Seranne, 1994), but they are also adequately explained as a result of transtension (Dewey, 2002; Fossen et al., 2013; Krabbendam & Dewey, 1998). However, our observations are not in agreement with a simple model of progressive transtensional folding during exhumation. The tight upright folds formed due to strong extension-perpendicular shortening during internal necking within the amphibolite-facies crust, while the upper crustal levels experienced only weak extension-perpendicular shortening. This differential folding might just represent the actual mechanism of extension-perpendicular crustal flow that is predicted from 3-D numerical models of transtensional core-complex formation (Le Pourhiet et al., 2012). We interpret the high-grade extension-parallel folds as the structural expression of isostasy-driven Poiseuille-type flow in the deep crust that moved low-viscosity solid-state material from the north and south into the dome and hence as a less drastic case of the mechanism postulated for migmatite-cored MCCs (e.g., Kruckenberg et al., 2011; Rey et al., 2017; Roger et al., 2015). As an interesting side note, this kind of differential folding was already described by Wegmann (1935) and Haller (1956) in the Greenland Caledonides. Distinct deformation regimes in relation to different metamorphic

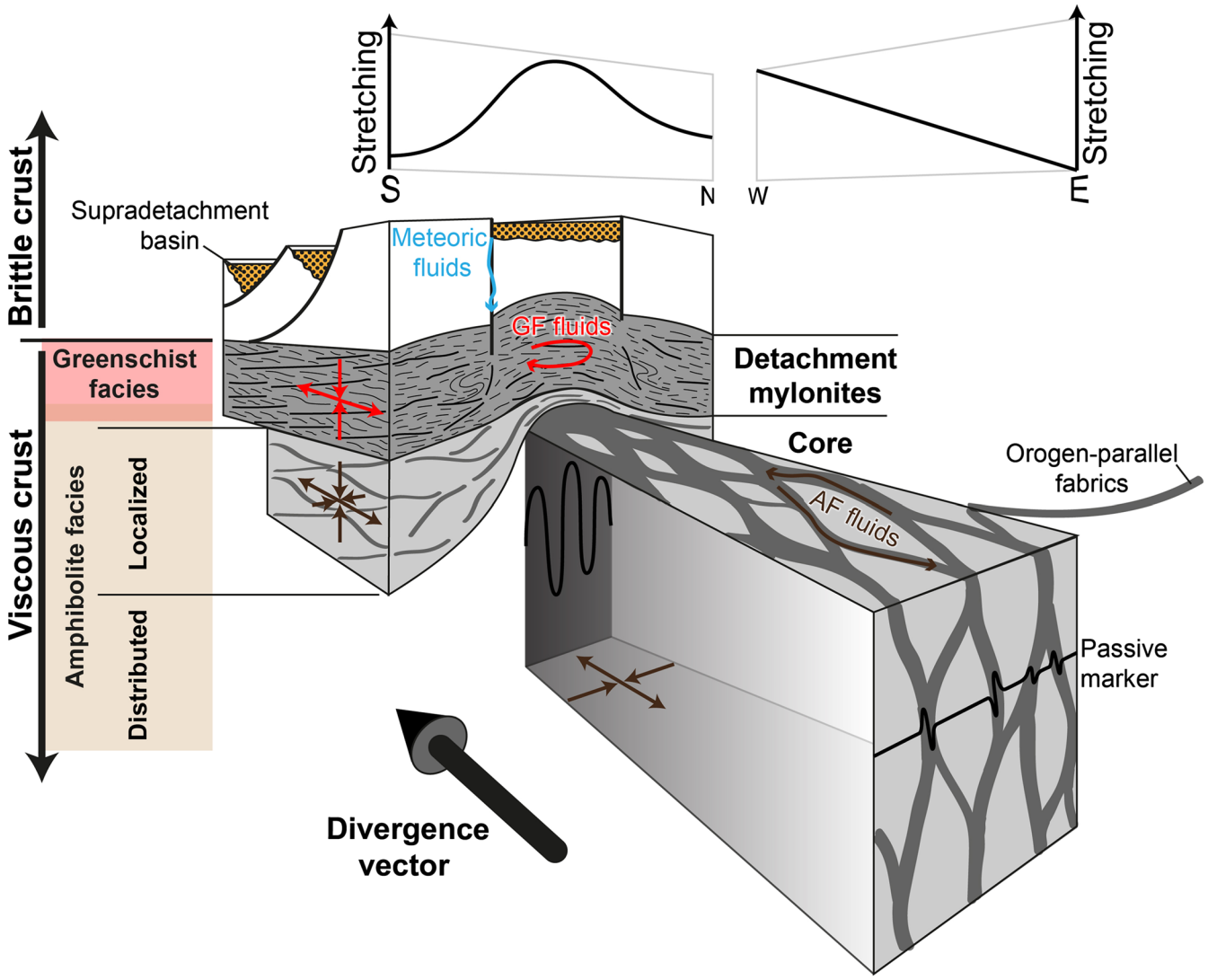

Figure 10. The internal structure of the Gulen MCC reveals a coherently stretched crustal section; however, distinct structural levels show very different deformation fabrics, kinematics, and fluids. Differences between these structural levels appear to relate to vertical metamorphic variations and horizontal strain gradients in N-S as well as E-W direction. Yet, they are all interpreted to have formed within the same kinematic boundary condition of sinistral transtension, which is represented by the divergence vector (Fossen et al., 2013). Below the brittle crust, the detachment mylonites show retrograde deformation from amphibolite-facies to semibrittle conditions, involving noncoaxial shearing and vertical shortening. The amphibolite-facies core consists of a domain of localized deformation, which is necked by pervasively sheared gneisses. The localized domain shows weak noncoaxial shearing and minor vertical shortening. In contrast, the distributed domain is characterized by coaxial shearing and N-S shortening.

conditions in vertical levels of the crust were the essence of the "stockwerk folding hypothesis." However, as pointed out by Wernicke (2009), these authors worked within a "fixist" paradigm that did not permit major horizontal movements. Therefore, it took many years until researchers realized that this "stockwerk folding" occurred in the footwall of massive extensional detachment shear zones (Hodges, 2016; White et al., 2002).

7.4. When Distant Relatives Become Close Neighbors: A Dynamic Model for Transtensional MCC Formation

During MCC exhumation, large parts of the original crust can be removed through the combination of incision, excision, and erosion. In the final structure of the Gulen MCC, syntectonic sedimentary rocks are directly juxtaposed with deep crustal levels, as demonstrated by the juxtaposition of the Fensfjorden Devonian basin with the eclogite-bearing crust across the BASZ. During the progressive evolution, material within the MCC is moving through different metamorphic conditions and deformation regimes, for

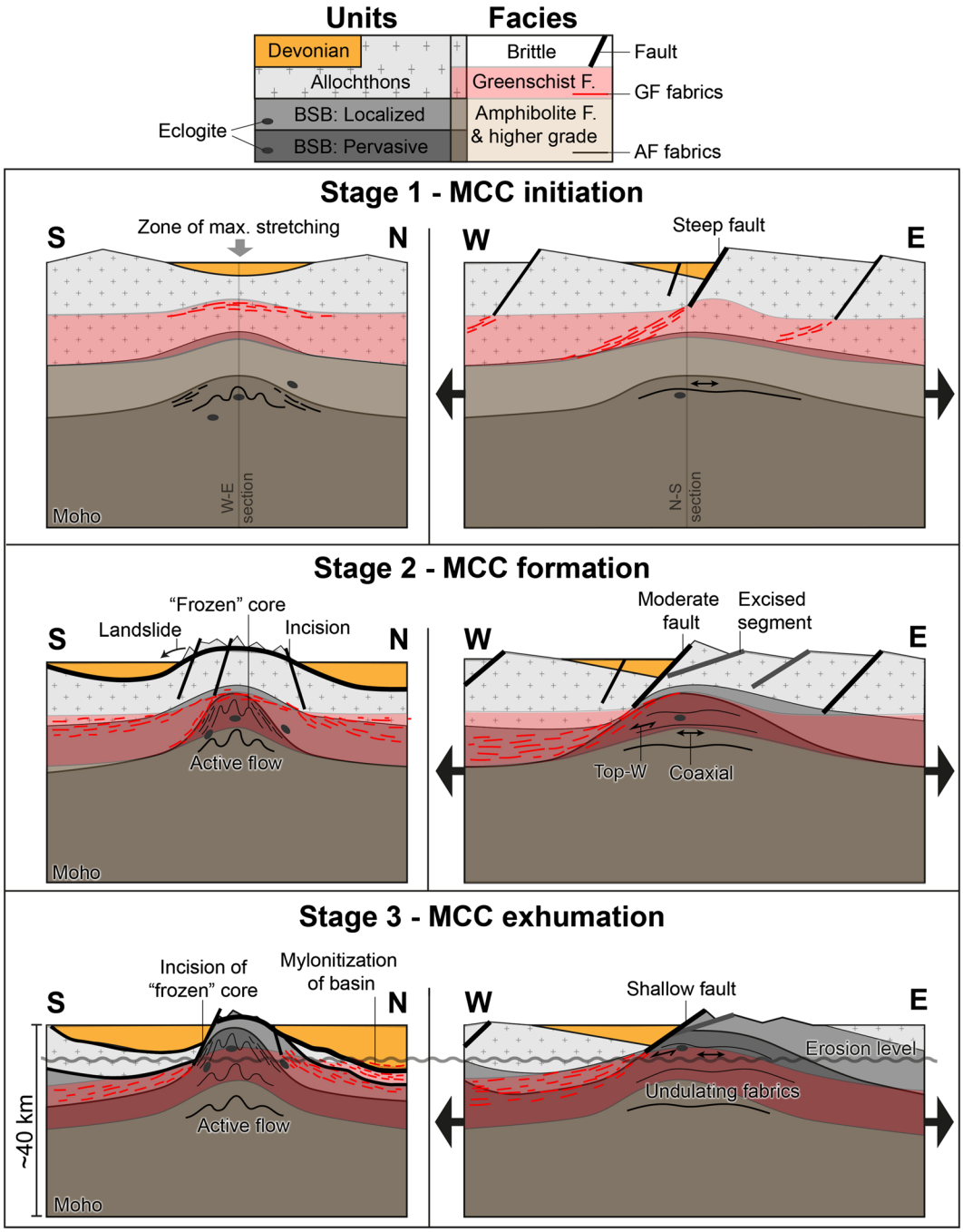

Figure 11. Sequential model for transtensional MCC formation in the footwall of the NSDZ. The evolution is illustrated in three stages with perpendicular cross sections that intersect each other in the center. The present erosion level is indicated in Stage 3. BSB = Baltic Shield basement (see text for discussion).

example, ductile rocks become brittle. In addition, the thermal conditions of the system are transient. Heat advection will change the geothermal gradient during MCC evolution (Whitney et al., 2013) and hence the spatial distribution of deformation regimes.

We incorporated these basic principles of MCC formation with existing models of postorogenic collapse of the Scandinavian Caledonides. Thereby we try to explain our field observations in accordance with the available information from other culminations of the WGR, the NSDZ, and recent work in the Devonian basins (Osmundsen & Péron-Pinvidic, 2018; Osmundsen et al., 2019). Our model is presented in Figure 11 as a

series of N-S and E-W cross sections to illustrate the 3-D kinematics. The time evolution is portrayed in three stages, which do not represent distinct phases but are an inevitable simplification made to illustrate the incremental evolution. The model that we come up with, of course, is highly simplified. We do not consider any internal structural geometries, rheological heterogeneities, or topographic variations that were possibly there at the end of Mode I extension. Our cross sections show neither E-W extension of the entire crust nor the associated extension-orthogonal shortening of the crustal section. Furthermore, we do not show the interference of different MCCs and the rotation of the divergence vector during progressive transtension.

Our model starts with a strongly thickened, horizontally layered crust. We show three rheological layers (Figure 11): brittle upper crust and the ductile crust separated between greenschist facies and amphibolite facies or higher grades. The crust consists of a thick pile of nappes overlaying the eclogite-bearing Baltic Shield basement (BSB). The unit boundaries serve only as passive markers for the structural evolution but do not represent rheological boundaries, except for the distinction between localized and pervasive deformation domains within the BSB. For reasons of simplicity, we overlap the greenschist-/amphibolite-facies boundary with the nappe-basement contact, but we note that extensional shearing in the lower nappes started at amphibolite-facies conditions (Johnston, Hacker, & Ducea, 2007b and references therein).

7.4.1. Stage 1: MCC Initiation

Initial extension formed steep, laterally limited normal faults that grade into mid-crustal shear zones at depth. Initial necking occurred at rheological transitions and involved extension-perpendicular folding within the amphibolite layer. It should be noted that both the depocenter of the initial basin and the future MCC formed in the center of the fault, because this is the zone of maximum stretching (e.g., Kapp et al., 2008; Osmundsen & Péron-Pinvidic, 2018; Osmundsen et al., 2019).

7.4.2. Stage 2: MCC Formation

During the main phase of MCC formation, the MCC started to rise in the zone of maximum stretching, and the basins were displaced to the flanks of the MCC as argued by Osmundsen et al. (2019). The synchronous formation of several MCCs along-strike (not shown in Figure 11) made the basins occupy synforms in between the rising antiforms. Different processes occurred at the different levels, which are still far apart from each other. The brittle crust, comprising the upper part of the nappe pile, was exposed, eroded, and deposited in the basins. Steep faults incised at the flanks of the MCC and form steep topography, which promoted catastrophic mass movements through large landslides as observed in the Solund and Kvamshesten basins (Hartz et al., 2002; Osmundsen et al., 1998). This shows that erosion can contribute significantly to upper crustal thinning during MCC exhumation.Greenschist facies top-to-W shearing within the detachment zone itself occurred mostly in the nappes, but as the upper crust was thinning progressively, also the BSB got involved. At the same time, at a deeper level, the amphibolite-facies crust was necking internally. Lateral inward flow occurred through extension-orthogonal shortening of the pervasively deforming low-viscosity crust. This process formed the high-grade core with steep strike-slip shear zones at its flanks. Differential exhumation at amphibolite-facies conditions is a consequence of this process. Rocks originating from different depths may be juxtaposed in relation to their position along major fold structures (compare position of eclogite bodies between stages 1 and 2). The high-grade core was exhumed progressively to greenschist facies conditions, but greenschist facies deformation was restricted to the top and the flanks of the culmination. Apparently, retrograde deformation stalled suddenly within the core, high-grade fabrics became “frozen-in,” and active flow moved to weaker layers.

A possible explanation for this may be that the internal necking of the ductile layer and the associated exhumation of the high-grade core represent a form of vertical heat advection. The rising core apparently contributed heat and fluids to the detachment system, which lead to weakening and increasing strain localization in the detachment layer. Furthermore, greenschist facies phyllonites, which formed previously through fluid-related retrogression within the detachment mylonites, are brought into the realm of brittle faulting. Such fault rocks with particularly low shear strength (Braathen et al., 2004), the abundance of fluids, and progressive heating within the detachment zone through head advection and possibly shear heating (Souche et al., 2013) imply that the brittle layer became weakened at this stage, promoting brittle faulting at progressively lower angles. At the same time, the rising core itself was cooling down, and therefore the active amphibolite-facies flow moved to a deeper and hotter level where the viscosity was lower. Furthermore, the possible occurrence of partial melting at a deeper, unexposed level of the MCC must be noted.

7.4.3. Stage 3: MCC Exhumation

The "frozen-in" high-grade core was exhumed progressively through localized deformation in the weakened detachment system. Brittle faulting occurred at progressively lower dips. At this stage, the deep crust had reached the surface and became eroded itself, as demonstrated by detrital Ar-Ar cooling ages from Hornelen basin (Templeton, 2015). The basins have reached a massive size at this stage, but only minor remnants are preserved at the present erosion level, which expose the oldest strata. Reconstructions imply a maximum basin depth between 9 and 13.5 km with a geothermal gradient of 38°C/km (Souche et al., 2012; Souche et al., 2013; Svensen et al., 2001). This implies that in parts of the system, the brittle crust had been entirely replaced by supradetachment basins. Devonian sediments were directly juxtaposed to detachment mylonites, and in the case of the Solund Basin, the lowest strata of the basin were even mylonitized themselves (Seranne & Seguret, 1987). At this stage, most of the nappe pile and even parts of the basement have been removed by ductile thinning, excision, and incision. The detachment system can be envisaged as a selective rock grinder: Weak rocks were smeared out ductilely in the detachment shear zone, while strong lithologies were removed through brittle faulting, footwall uplift, and erosion. In the synforms of the detachment zone, we find mostly weak rheologies like mica schists and phyllonites preserved. At the flank of the MCC, steep strike-slip faults incised the core and exploited previously formed ductile fabrics. In the case of the BASZ, the basin was directly juxtaposed to the deep crust. Further isostatic compensation may have occurred through folding at deeper amphibolite-facies levels.

At the end of this evolution, our reconstruction implies a crustal thickness of around 40 km (10 km thick basin fill + 30 km present crustal thickness). Final juxtaposition of the different units occurred through brittle fault reactivation during North Sea rifting (e.g., Eide et al., 1997; Torsvik et al., 1992).

8. Conclusions and Implications for Postorogenic Exhumation of (Ultra-)High-Pressure Rocks

Our study shows that vertical metamorphic variations and lateral strain gradients during postorogenic transtension may cause a highly variable behavior of the crust, leading to differential exhumation and the formation of MCCs. We think that our field-based model (Figure 11) encapsulates important general aspects of MCC formation in 3-D strain settings and can contribute to understand MCCs where the deep levels of the crust are not exposed. Large magnitudes of extension can amplify differential extension-orthogonal shortening of distinct crustal levels. This process results in characteristic fold structures, which resemble the historic "stockwerk folding hypothesis" (Wernicke, 2009) and might easily be mistaken for contractional structures formed during convergence. In the case of the WGR, however, they clearly formed during postorogenic transtension. Thus, like in the case of migmatite-cored MCCs (Rey et al., 2017), extension-orthogonal contraction within the deep crust is the main mechanism of isostasy-driven crustal flow also in solid-state MCCs.

This crustal flow mechanism has the potential to redistribute material within the extending crust (Figure 11). Hence, it might be highly important for the exhumation of (ultra-) high-pressure rocks in postorogenic settings. A comprehensive look at the WGR demonstrates that this might have been the case in the Caledonides. The Gulen MCC is the southernmost of a series of evenly spaced MCCs (Figures 1A and 1B); however, also the ultrahigh-pressure domains north of the Hornelen Basin have similar orientations, spacing, and wavelengths. If the pressure estimates from these rocks reflect burial depth, the occurrence of such discrete domains (e.g., Root et al., 2005) implies that the rocks inside these domains have been exhumed from greater depth than the rocks in the surrounding areas. We suggest that our model of crustal flow could offer a plausible explanation for this differential exhumation pattern. This would imply that the processes across the WGR have been self-similar over large areas of the giant high-pressure terrane.

Even if we zoom out to the scale of the entire orogen, we can find notable self-similarities. Already Ramberg (1981) pointed out the existence of two distinct belts of basement domes that run parallel along the entire length of the Scandinavian Caledonides. Osmundsen et al. (2005) showed that these domes can be seen as different types of MCCs. The belt in the foreland consists of cylindrical domes with long axes perpendicular to the extension direction, which comprise low-grade metamorphic rocks and record low amounts of exhumation. In contrast, the domes in the hinterland of the orogen are noncylindrical with long axes parallel to

the extension direction and expose high-grade metamorphic rocks, which were exhumed from great depth. The different shapes of these domes resemble exactly the a-type versus b-type classification that has been suggested for Aegean domes (Jolivet et al., 2004). Le Pourhiet et al. (2012) attributed the coeval formation of both dome types in the Cyclades to distinct kinematic boundary conditions related to a slab tear during rollback of the Aegean slab. In the case of the Scandinavian Caledonides, however, the different dome-types appear systematically with respect to their position toward the foreland or the hinterland of the orogen. Furthermore, as they occur along the entire length of the orogen, the domes in the Scandinavian Caledonides are likely to have formed within the same kinematic boundary conditions. Thus, the different dome types apparently relate to variations in metamorphic conditions at the onset of extension, as well as different amounts of crustal stretching and associated exhumation. At least in the case of the Scandinavian domes, noncylindricality appears to be a function of crustal stretching, but we speculate that this relationship might also apply universally. During the formation of large normal-fault systems, there will always be along-strike variations, which can trigger differential crustal flow in the deep crust. This creates a feedback loop that can be amplified during progressive crustal stretching. Hence, an alternative explanation for the coeval formation of a- and b-type domes might be that noncylindrical MCCs will be exhumed from the deep crust if a critical amount of extension is reached (Stage 2 in Figure 13). A way to test this hypothesis could be to analyze systematic variations in metamorphic grade and exhumation recorded in a- and b-type domes around the world, respectively.

Acknowledgments
The field data from this study can be accessed online (https://doi.org/10.6084/m9.figshare.c.4697006.v1). JDW thanks Sebastian Wolf, Arne Fuhrmann, Thilo Wrona, Theo Kassaras, and Anne Reiff for their company that made fieldwork possible. We thank Irina Dumitru and Irene Heggstad at UiB for help with sample preparation and BSE imaging. This research was funded by VISTA—a basic research program in collaboration between the Norwegian Academy of Science and Letters and Equinor [grant number 6271] as well as a student grant for JDW from the Meltzer fond at the University of Bergen. We thank C. Teyssier and P. Rey for constructive reviews and L. Jolivet and W. Behr for editorial handling.

References

Andersen, T. B., & Jamtveit, B. (1990). Uplift of deep crust during orogenic extensional collapse: A model based on field studies in the Sogn-Sunnfjord Region of Western Norway. *Tectonics*, *9*(5), 1097–1111. https://doi.org/10.1029/TC009i005p01097

Andersen, T. B., Jamtveit, B., Dewey, J. F., & Swensson, E. (1991). Subduction and eduction of continental crust: Major mechanisms during continent-continent collision and orogenic extensional collapse, a model based on the South Norwegian Caledonides. *Terra Nova*, *3*(3), 303–310. https://doi.org/10.1111/j.1365-3121.1991.tb00148.x

Andersen, T. B., Osmundsen, P. T., & Jolivet, L. (1994). Deep crustal fabrics and a model for the extensional collapse of the southwest Norwegian Caledonides. *Journal of Structural Geology*, *16*(9), 1191–1203. https://doi.org/10.1016/0191-8141(94)90063-9

Austrheim, H., Erambert, M., & Engvik, A. K. (1997). Processing of crust in the root of the Caledonian continental collision zone: The role of eclogitization. *Tectonophysics*, *273*(1-2), 129–153. https://doi.org/10.1016/S0040-1951(96)00291-0

Bingen, B., Skar, O., Marker, M., Sigmond, E. M. O., Nordgulen, O., Ragnhildstveit, J., et al. (2005). Timing of continental building in the Sveconorwegian orogen, SW Scandinavia. *Norwegian Journal of Geology*, *85*(1-2), 87–116.

Block, L., & Royden, L. H. (1990). Core complex geometries and regional scale flow in the lower crust. *Tectonics*, *9*(4), 557–567. https://doi.org/10.1029/TC009i004p00557

Boundy, T. M., Essene, E. J., Hall, C. M., Austrheim, H., & Halliday, A. N. (1996). Rapid exhumation of lower crust during continent-continent collision and late extension: Evidence from Ar-40/Ar-39 incremental heating of hornblendes and muscovites, Caledonian orogen, western Norway. *Geological Society of America Bulletin*, *108*(11), 1425–1437. https://doi.org/10.1130/0016-7606(1996)108

Braathen, A., & Erambert, M. (2014). Structural and metamorphic history of the Engebøfjellet Eclogite and the exhumation of the Western Gneiss Region, Norway. *Norwegian Journal of Geology*, *94*, 53–76.

Braathen, A., Osmundsen, P. T., & Gabrielsen, R. H. (2004). Dynamic development of fault rocks in a crustal-scale detachment: An example from western Norway. *Tectonics*, *23*, n/a. https://doi.org/10.1029/2003tc001558

Brueckner, H. K. (2018). The great eclogite debate of the Western Gneiss Region, Norwegian Caledonides: The in situ crustal v. exotic mantle origin controversy. *Journal of Metamorphic Geology*, *36*(5), 517–527. https://doi.org/10.1111/jmg.12314

Brun, J.-P., Sokoutis, D., Tirel, C., Gueydan, F., Van Den Driessche, J., & Beslier, M.-O. (2017). Crustal versus mantle core complexes. *Tectonophysics*, *746*, 22–45. https://doi.org/10.1016/j.tecto.2017.09.017

Buck, W. R. (1991). Modes of continental lithospheric extension. *Journal of Geophysical Research*, *96*(B12), 20,161–20,178. https://doi.org/10.1029/91jb01485

Butler, J. P., Beaumont, C., & Jamieson, R. A. (2015). Paradigm lost: Buoyancy thwarted by the strength of the Western Gneiss Region (ultra) high-pressure terrane, Norway. *Lithosphere*, *7*(4), 379–407. https://doi.org/10.1130/L426.1

Butler, J. P., Jamieson, R. A., Dunning, G. R., Pecha, M. E., Robinson, P., & Steenkamp, H. M. (2018). Timing of metamorphism and exhumation in the Nordøyane ultra-high-pressure domain, Western Gneiss Region, Norway: New constraints from complementary CA-ID-TIMS and LA-MC-ICP-MS geochronology. *Lithos*, *310-311*, 153–170. https://doi.org/10.1016/j.lithos.2018.04.006

Chauvet, A., & Dallmeyer, R. D. (1992). 40Ar/39Ar mineral dates related to Devonian extension in the southwestern Scandinavian Caledonides. *Tectonophysics*, *210*(1-2), 155–177. https://doi.org/10.1016/0040-1951(92)90133-Q

Chauvet, A., & Seranne, M. (1994). Extension-parallel folding in the Scandinavian Caledonides: Implications for late-orogenic processes. *Tectonophysics*, *238*(1-4), 31–54. https://doi.org/10.1016/0040-1951(94)90048-5

Coint, N., Slagstad, T., Roberts, N. M. W., Marker, M., Rohr, T., & Sorensen, B. E. (2015). The Late Mesoproterozoic Sirdal Magmatic Belt, SW Norway: Relationships between magmatism and metamorphism and implications for Sveconorwegian orogenesis. *Precambrian Research*, *265*, 57–77. https://doi.org/10.1016/j.precamres.2015.05.002

Coney, P. J. (1980). Cordilleran metamorphic core complexes: An overview. *Geological Society of America Memoirs*, *153*, 7–31. https://doi.org/10.1130/MEM153-p7

Cooper, F. J., Platt, J. P., & Behr, W. M. (2017). Rheological transitions in the middle crust: insights from Cordilleran metamorphic core complexes. *Solid Earth*, *8*(1), 199–215. https://doi.org/10.5194/se-8-199-2017

Cuthbert, S. J., Carswell, D. A., Krogh-Ravna, E. J., & Wain, A. (2000). Eclogites and eclogites in the Western Gneiss Region, Norwegian Caledonides. *Lithos*, *52*(1-4), 165–195. https://doi.org/10.1016/S0024-4937(99)00090-0

Cutts, J. A., M. A. Smit, E. Kooijman, and M. Schmitt (2019), Two-stage cooling and exhumation of deeply subducted continents, *Tectonics*, *38*(0), doi: https://doi.org/10.1029/2018tc005292, 3, 863, 877.
Dewey, J. F. (2002). Transtension in arcs and orogens. *International Geology Review*, *44*(5), 402–439. https://doi.org/10.2747/0020-6814.44.5.402
Duclaux, G., Rey, P., Guillot, S., & Ménot, R.-P. (2007). Orogen-parallel flow during continental convergence: Numerical experiments and Archean field examples. *Geology*, *35*, 715–718. https://doi.org/10.1130/g23540a.1
Eide, E. A., Haabesland, N. E., Osmundsen, P. T., Andersen, T. B., Roberts, D., & Kendrick, M. A. (2005). Modern techniques and Old Red problems: Determining the age of continental sedimentary deposits with Ar-40/Ar-39 provenance analysis in west-central Norway. *Norwegian Journal of Geology*, *85*(1-2), 133–149.
Eide, E. A., Torsvik, T. H., & Andersen, T. B. (1997). Absolute dating of brittle fault movements: Late Permian and late Jurassic extensional fault breccias in western Norway. *Terra Nova*, *9*(3), 135–139. https://doi.org/10.1046/j.1365-3121.1997.d01-21.x
Engvik, A. K., Austrheim, H., & Andersen, T. B. (2000). Structural, mineralogical and petrophysical effects on deep crustal rocks of fluid-limited polymetamorphism, Western Gneiss Region, Norway. *Journal of the Geological Society*, *157*(1), 121–134. https://doi.org/10.1144/jgs.157.1.121
Engvik, A. K., Willemoes-Wissing, B., & Lutro, O. (2018). High-temperature, decompressional equilibration of the eclogite facies orogenic root (Western Gneiss Region, Norway). *Journal of Metamorphic Geology*, *36*(5), 529–545. https://doi.org/10.1111/jmg.12418
Fossen, H. (1992). The role of extensional tectonics in the Caledonides of South Norway. *Journal of Structural Geology*, *14*(8-9), 1033–1046. https://doi.org/10.1016/0191-8141(92)90034-T
Fossen, H. (2010). Extensional tectonics in the North Atlantic Caledonides: A regional view. *Geological Society, London, Special Publications*, *335*(1), 767–793. https://doi.org/10.1144/SP335.31
Fossen, H., Teyssier, C., & Whitney, D. L. (2013). Transtensional folding. *Journal of Structural Geology*, *56*, 89–102. https://doi.org/10.1016/j.jsg.2013.09.004
Ganzhorn, A. C., Labrousse, L., Prouteau, G., Leroy, C., Vrijmoed, J. C., Andersen, T. B., & Arbaret, L. (2014). Structural, petrological and chemical analysis of syn-kinematic migmatites: insights from the Western Gneiss Region, Norway. *Journal of Metamorphic Geology*, *32*(6), 647–673. https://doi.org/10.1111/jmg.12084
Gordon, S. M., Whitney, D. L., Teyssier, C., & Fossen, H. (2013). U-Pb dates and trace-element geochemistry of zircon from migmatite, Western Gneiss Region, Norway: Significance for history of partial melting in continental subduction. *Lithos*, *170-171*, 35–53. https://doi.org/10.1016/j.lithos.2013.02.003
Griffin, W. L., & Brueckner, H. K. (1980). Caledonian Sm-Nd ages and a crustal origin for Norwegian eclogites. *Nature*, *285*(5763), 319–321. https://doi.org/10.1038/285319a0
Hacker, B. R., Andersen, T. B., Johnston, S., Kylander-Clark, A. R. C., Peterman, E. M., Walsh, E. O., & Young, D. (2010). High-temperature deformation during continental-margin subduction & exhumation: The ultrahigh-pressure Western Gneiss Region of Norway. *Tectonophysics*, *480*(1-4), 149–171. https://doi.org/10.1016/j.tecto.2009.08.012
Hacker, B. R., Andersen, T. B., Root, D. B., Mehl, L., Mattinson, J. M., & Wooden, J. L. (2003). Exhumation of high-pressure rocks beneath the Solund Basin, Western Gneiss Region of Norway. *Journal of Metamorphic Geology*, *21*(6), 613–629. https://doi.org/10.1046/j.1525-1314.2003.00468.x
Hacker, B. R., Kylander-Clark, A. R. C., Holder, R., Andersen, T. B., Peterman, E. M., Walsh, E. O., & Munnikhuis, J. K. (2015). Monazite response to ultrahigh-pressure subduction from U-Pb dating by laser ablation split stream. *Chemical Geology*, *409*, 28–41. https://doi.org/10.1016/j.chemgeo.2015.05.008
Haller, J. (1956). Probleme der Tiefentektonik Bauformen im Migmatit Stockwerk der Ostgrönländischen Kaledoniden. *Geol Rundsch*, *45*(2), 159–167. https://doi.org/10.1007/BF01802002
Hartz, E. H., Martin, M. W., Andresen, A., & Andersen, T. B. (2002). Volcanic rocks in the Devonian Solund Basin, Western Norway: Large landslides of Silurian (439 Ma) rhyolites. *Journal of the Geological Society*, *159*(2), 121–128. https://doi.org/10.1144/0016-764901-063
Hodges, K. V. (2016). Crustal decoupling in collisional orogenesis: Examples from the East Greenland Caledonides and Himalaya. *Annu Rev Earth Pl Sc*, *44*(1), 685–708. https://doi.org/10.1146/annurev-earth-060115-012412
Holder, R. M., Hacker, B. R., Kylander-Clark, A. R. C., & Cottle, J. M. (2015). Monazite trace-element and isotopic signatures of (ultra)high-pressure metamorphism: Examples from the Western Gneiss Region, Norway. *Chemical Geology*, *409*, 99–111. https://doi.org/10.1016/j.chemgeo.2015.04.021
Johnston, S., Hacker, B. R., & Ducea, M. N. (2007). Exhumation of ultrahigh-pressure rocks beneath the Hornelen segment of the Nordfjord-Sogn Detachment Zone, western Norway. *GSA Bulletin*, *119*(9-10), 1232–1248. https://doi.org/10.1130/B26172.1
Johnston, S. M., Hacker, B. R., & Andersen, T. B. (2007). Exhuming Norwegian ultrahigh-pressure rocks: Overprinting extensional structures and the role of the Nordfjord-Sogn Detachment Zone. *Tectonics*, *26*, n/a. https://doi.org/10.1029/2005TC001933
Jolivet, L., Famin, V., Mehl, C., Parra, T., Aubourg, C., Hebert, R., & Philippot, P. (2004). Strain localization during crustal-scale boudinage to form extensional metamorphic domes in the Aegean Sea. *Geol Soc Am Spec Pap*, *380*, 185–210. https://doi.org/10.1130/0-8137-2380-9.185
Kapp, P., Stockli, D., Taylor, M., & Ding, L. (2008). Development of active low-angle normal fault systems during orogenic collapse: Insight from Tibet. *Geology*, *36*(1), 7–10. https://doi.org/10.1130/g24054a.1
Kildal, E. S. (1970). Geologisk kart over Norge, berggrunnskart, Måløy, 1:250.000, norsk utgave. *Norges geologiske undersøkelse.*
Kohn, M. J., Corrie, S. L., & Markley, C. (2015). The fall and rise of metamorphic zircon. *Am Mineral*, *100*(4), 897–908. https://doi.org/10.2138/am-2015-5064
Krabbendam, M., & Dewey, J. F. (1998). Exhumation of UHP rocks by transtension in the Western Gneiss Region, Scandinavian Caledonides. *Geological Society, London, Special Publications*, *135*(1), 159–181. https://doi.org/10.1144/GSL.SP.1998.135.01.11
Kruckenberg, S. C., Vanderhaeghe, O., Ferre, E. C., Teyssier, C., & Whitney, D. L. (2011). Flow of partially molten crust and the internal dynamics of a migmatite dome, Naxos, Greece. *Tectonics*, *30*, n/a. https://doi.org/10.1029/2010tc002751
Kylander-Clark, A. R. C., & Hacker, B. R. (2014). Age and significance of felsic dikes from the UHP western gneiss region. *Tectonics*, *33*, 2342–2360. https://doi.org/10.1002/2014TC003582
Kylander-Clark, A. R. C., Hacker, B. R., & Mattinson, J. M. (2008). Slow exhumation of UHP terranes: Titanite and rutile ages of the Western Gneiss Region, Norway. *Earth and Planetary Science Letters*, *272*(3-4), 531–540. https://doi.org/10.1016/j.epsl.2008.05.019
Labrousse, L., Prouteau, G., & Ganzhorn, A.-C. (2011). Continental exhumation triggered by partial melting at ultrahigh pressure. *Geology*, *39*(12), 1171–1174. https://doi.org/10.1130/g32316.1
Le Pourhiet, L., Huet, B., May, D. A., Labrousse, L., & Jolivet, L. (2012). Kinematic interpretation of the 3D shapes of metamorphic core complexes. *Geochem., Geophy., Geosy.*, *13*(9). https://doi.org/10.1029/2012GC004271

McClay, M., Norton, G., Coney, P., & Davis, G. H. (1986). Collapse of the Caledonian orogen and the Old Red Sandstone. *Nature*, *323*(6084), 147–149. https://doi.org/10.1038/323147a0

Milnes, A., Wennberg, O., Skår, Ø., & Koestler, A. (1997). Contraction, extension and timing in the South Norwegian Caledonides: The Sognefjord transect. *Geological Society, London, Special Publications*, *121*(1), 123–148. https://doi.org/10.1144/GSL.SP.1997.121.01.06

Milnes, A. G., & Koyi, H. A. (2000). Ductile rebound of an orogenic root: Case study and numerical model of gravity tectonics in the Western Gneiss Complex, Caledonides, southern Norway. *Terra Nova*, *12*(1), 1–7. https://doi.org/10.1046/j.1365-3121.2000.00266.x

Osmundsen, A., Markussen, & Svendby (1998). Tectonics and sedimentation in the hangingwall of a major extensional detachment: The Devonian Kvamshesten Basin, western Norway. *Basin Research*, *10*(2), 213–234. https://doi.org/10.1046/j.1365-2117.1998.00064.x

Osmundsen, P. T., & Andersen, T. B. (2001). The middle Devonian basins of western Norway: Sedimentary response to large-scale trans-tensional tectonics? *Tectonophysics*, *332*(1-2), 51–68. https://doi.org/10.1016/S0040-1951(00)00249-3

Osmundsen, P. T., Braathen, A., Sommaruga, A., Skilbrei, J. R., Nordgulen, O., Roberts, D., et al. (2005). Metamorphic core complexes and gneiss-cored culminations along the mid-Norwegian margin: An overview and some current ideas. *Norwegian Petroleum Society Special Publications*, *12*, 29–41. https://doi.org/10.1016/S0928-8937(05)80042-6

Osmundsen, P. T., Braathen, A., Svendby, A. K., Midtkandal, I., More, M. P., & Andersen, T. B. (2019). *On fault growth and orthogonal shortening in transtensional supradetachment basins, paper presented at 49th TSG Annual Meeting*. Bergen: Tectonic Studies Group.

Osmundsen, P. T., & Péron-Pinvidic, G. (2018). Crustal-scale fault interaction at rifted margins and the formation of domain-bounding breakaway complexes: Insights from offshore Norway. *Tectonics*, *37*(3), 935–964. https://doi.org/10.1002/2017tc004792

Platt, J. P., Behr, W. M., & Cooper, F. J. (2015). Metamorphic core complexes: Windows into the mechanics and rheology of the crust. *Journal of the Geological Society*, *172*(1), 9–27. https://doi.org/10.1144/jgs2014-036

Ragnhildstveit, J., & Helliksen, D. (1997). Geologisk kart over Norge, berggrunnskart Bergen - M 1:250.000. *Norges Geologiske Undersøkelse*.

Ramberg, H. (1981). The role of gravity in orogenic belts. *Geological Society, London, Special Publications*, *9*(1), 125–140. https://doi.org/10.1144/GSL.SP.1981.009.01.11

Rey, P. F., Mondy, L., Duclaux, G., Teyssier, C., Whitney, D. L., Bocher, M., & Prigent, C. (2017). The origin of contractional structures in extensional gneiss domes. *Geology*, *45*(3), 263–266. https://doi.org/10.1130/G38595.1

Rey, P. F., Teyssier, C., Kruckenberg, S. C., & Whitney, D. L. (2011). Viscous collision in channel explains double domes in metamorphic core complexes. *Geology*, *39*(4), 387–390. https://doi.org/10.1130/G31587.1

Rey, P. F., Teyssier, C., & Whitney, D. L. (2009). The role of partial melting and extensional strain rates in the development of metamorphic core complexes. *Tectonophysics*, *477*(3-4), 135–144. https://doi.org/10.1016/j.tecto.2009.03.010

Roger, F., Teyssier, C., Respaut, J. P., Rey, P. F., Jolivet, M., Whitney, D. L., et al. (2015). Timing of formation and exhumation of the Montagne Noire double dome, French Massif Central. *Tectonophysics*, *640-641*, 53–69. https://doi.org/10.1016/j.tecto.2014.12.002

Røhr, T. S., Corfu, F., Austrheim, H., & Andersen, T. B. (2004). Sveconorwegian U-Pb zircon and monazite ages of granulite-facies rocks, Hisarøya, Gulen, Western Gneiss Region, Norway. *Norwegian Journal of Geology*, *84*(4), 251–256.

Root, D. B., Hacker, B. R., Gans, P. B., Ducea, M. N., Eide, E. A., & Mosenfelder, J. L. (2005). Discrete ultrahigh-pressure domains in the Western Gneiss Region, Norway: Implications for formation and exhumation. *Journal of Metamorphic Geology*, *23*(1), 45–61. https://doi.org/10.1111/j.1525-1314.2005.00561.x

Seranne, M., & Seguret, M. (1987). The Devonian basins of western Norway: Tectonics and kinematics of an extending crust. *Geological Society, London, Special Publications*, *28*(1), 537–548. https://doi.org/10.1144/GSL.SP.1987.028.01.35

Slagstad, T., Roberts, N. M. W., Coint, N., Høy, I., Sauer, S., Kirkland, C. L., et al. (2018). Magma-driven, high-grade metamorphism in the Sveconorwegian Province, southwest Norway, during the terminal stages of Fennoscandian Shield evolution. *Geosphere*, *14*(2), 861–882. https://doi.org/10.1130/ges01565.1

Souche, A., Beyssac, O., & Andersen, T. B. (2012). Thermal structure of supra-detachment basins: A case study of the Devonian basins of western Norway. *Journal of the Geological Society*, *169*(4), 427–434. https://doi.org/10.1144/0016-76492011-155

Souche, A., Medvedev, S., Andersen, T. B., & Dabrowski, M. (2013). Shear heating in extensional detachments: Implications for the thermal history of the Devonian basins of W Norway. *Tectonophysics*, *608*, 1073–1085. https://doi.org/10.1016/j.tecto.2013.07.005

Spencer, K. J., Hacker, B. R., Kylander-Clark, A. R. C., Andersen, T. B., Cottle, J. M., Stearns, M. A., et al. (2013). Campaign-style titanite U-Pb dating by laser-ablation ICP: Implications for crustal flow, phase transformations and titanite closure. *Chemical Geology*, *341*, 84–101. https://doi.org/10.1016/j.chemgeo.2012.11.012

Svensen, H., Jamtveit, B., Banks, D. A., & Karlsen, D. (2001). Fluids and halogens at the diagenetic-metamorphic boundary: Evidence from veins in continental basins, western Norway. *Geofluids*, *1*(1), 53–70. https://doi.org/10.1046/j.1468-8123.2001.11003.x

Templeton, J. A. (2015). *Structural evolution of the Hornelen Basin (Devonian, Norway) from detrital thermochronology* (243 pp.). New York: Columbia University.

Torsvik, T. H., Sturt, B. A., Swensson, E., Andersen, T. B., & Dewey, J. F. (1992). Palaeomagnetic dating of fault rocks: Evidence for Permian and Mesozoic movements and brittle deformation along the extensional Dalsfjord Fault, western Norway. *Geophys J Int*, *109*(3), 565–580. https://doi.org/10.1111/j.1365-246X.1992.tb00118.x

Vanderhaeghe, O., & Teyssier, C. (2001). Partial melting and flow of orogens. *Tectonophysics*, *342*(3-4), 451–472. https://doi.org/10.1016/S0040-1951(01)00175-5

Vrijmoed, J. C., Podladchikov, Y. Y., Andersen, T. B., & Hartz, E. H. (2009). An alternative model for ultra-high pressure in the Svartberget Fe-Ti garnet-peridotite, Western Gneiss Region, Norway. *Eur J Mineral*, *21*(6), 1119–1133. https://doi.org/10.1127/0935-1221/2009/0021-1985

Walsh, E. O., Hacker, B. R., Gans, P. B., Grove, M., & Gehrels, G. (2007). Protolith ages and exhumation histories of (ultra)high-pressure rocks across the Western Gneiss Region, Norway. *Geological Society of America Bulletin*, *119*(3-4), 289–301. https://doi.org/10.1130/B25817.1

Walsh, E. O., Hacker, B. R., Gans, P. B., Wong, M. S., & Andersen, T. B. (2013). Crustal exhumation of the Western Gneiss Region UHP terrane, Norway: 40Ar/39Ar thermochronology and fault-slip analysis. *Tectonophysics*, *608*, 1159–1179. https://doi.org/10.1016/j.tecto.2013.06.030

Wegmann, C. E. (1935). Zur Deutung der Migmatite. *Geol Rundsch*, *26*(5), 305–350. https://doi.org/10.1007/BF01802849

Wennberg, O. P., Milnes, A. G., & Winsvold, I. (1998). The northern Bergen Arc shear zone: An oblique-lateral ramp in the Devonian extensional detachment system of western Norway. *Norwegian Journal of Geology*, *78*(3), 169–184.

Wernicke, B. (2009). The detachment era (1977–1982) and its role in revolutionizing continental tectonics. *Geological Society, London, Special Publications*, *321*(1), 1–8. https://doi.org/10.1144/sp321.1

White, A. P., Hodges, K. V., Martin, M. W., & Andresen, A. (2002). Geologic constraints on middle-crustal behavior during broadly synorogenic extension in the central East Greenland Caledonides. *Int J Earth Sci*, *91*(2), 187–208. https://doi.org/10.1007/s005310100227

Whitney, D. L., Teyssier, C., Rey, P., & Buck, W. R. (2013). Continental and oceanic core complexes. *Geological Society of America Bulletin*, *125*(3-4), 273–298. https://doi.org/10.1130/B30754.1

Wiest, J. D., Jacobs, J., Fossen, H., & Osmundsen, P. T. (2019). *Shearing, folding and retrogression during exhumation of the southernmost culmination of the Western Gneiss Region, Gulen, SW Norway, paper presented at Geological Society of Norway 33rd Geological winter meeting*. Bergen: Geological Society of Norway.

Wiest, J. D., Jacobs, J., Ksienzyk, A. K., & Fossen, H. (2018). Sveconorwegian vs. Caledonian orogenesis in the eastern Øygarden Complex, SW Norway—Geochronology, structural constraints and tectonic implications. *Precambrian Research*, *305*, 1–18. https://doi.org/10.1016/j.precamres.2017.11.020

Winsvold, I. (1996). *Tektonisk utvikling av Byrknesøy (Vest-Norge) - opphevingshistorie av eklogitter i sørvestlige del av Vestre Gneiskompleks*. Bergen Norway: University of Bergen.

Young, D. J., Hacker, B. R., Andersen, T. B., & Gans, P. B. (2011). Structure and $^{40}Ar/^{39}Ar$ thermochronology of an ultrahigh-pressure transition in western Norway. *Journal of the Geological Society*, *168*(4), 887–898. https://doi.org/10.1144/0016-76492010-075